



This discussion paper is/has been under review for the journal Atmospheric Measurement Techniques (AMT). Please refer to the corresponding final paper in AMT if available.

# Tropospheric column amount of ozone retrieved from SCIAMACHY limb-nadir-matching observations

F. Ebojie<sup>1</sup>, C. von Savigny<sup>1,\*</sup>, A. Ladstätter-Weißenmayer<sup>1</sup>, A. Rozanov<sup>1</sup>, M. Weber<sup>1</sup>, K. Eichmann<sup>1</sup>, S. Bötel<sup>1</sup>, N. Rahpoe<sup>1</sup>, H. Bovensmann<sup>1</sup>, and J. P. Burrows<sup>1</sup>

<sup>1</sup>Institute of Environmental Physics (IUP), University of Bremen, P.O. Box 330440, 28334 Bremen, Germany

\*now at: Institute of Physics, Ernst-Moritz-Arndt-University of Greifswald, Felix-Hausdorff-Str. 6, 17489 Greifswald, Germany

Received: 31 July 2013 – Accepted: 20 August 2013 – Published: 27 August 2013

Correspondence to: F. Ebojie (felix@iup.physik.uni-bremen.de)

Published by Copernicus Publications on behalf of the European Geosciences Union.

AMTD

6, 7811–7865, 2013

Tropospheric ozone retrievals from SCIAMACHY observations

F. Ebojie et al.

Title Page

Abstract

Introduction

Conclusions

References

Tables

Figures

◀

▶

Back

Close

Full Screen / Esc

Printer-friendly Version

Interactive Discussion



## Abstract

Tropospheric ozone, O<sub>3</sub>, has two sources: transport from the stratosphere and photochemical production in the troposphere. It plays important roles in atmospheric chemistry and climate change. In this manuscript we describe the retrieval of tropospheric O<sub>3</sub> columns from limb-nadir matching (LNM) observations of the SCanning Imaging Absorption spectroMeter for Atmospheric CHartographY (SCIAMACHY) instrument, which flies as part of the payload onboard the European Space Agency (ESA) satellite Envisat. This retrieval technique is a residual approach that utilizes the subtraction of the stratospheric O<sub>3</sub> columns, derived from the limb observations, from the total O<sub>3</sub> columns, derived from the nadir observations. The technique requires accurate knowledge of the stratospheric O<sub>3</sub> columns, the total O<sub>3</sub> columns, tropopause height, and their associated errors. The stratospheric O<sub>3</sub> columns were determined from the stratospheric O<sub>3</sub> profile retrieved in the Hartley and Chappius bands, based on SCIAMACHY limb scattering measurements. The total O<sub>3</sub> columns were also derived from SCIAMACHY measurements, in the nadir viewing mode using the Weighting Function Differential Optical Absorption Spectroscopy (WFDOAS) technique in the Huggins band. Comparisons of the tropospheric O<sub>3</sub> columns from SCIAMACHY and collocated measurements from ozonesondes, in both hemispheres between January 2003 and December 2011 show agreement to within 2–5 DU (1 DU =  $2.69 \times 10^{16}$  molecules cm<sup>-2</sup>). Comparison of tropospheric O<sub>3</sub> from SCIAMACHY with the results from ozonesondes, the Tropospheric Emission Spectrometer (TES), and the LNM method combining Ozone Monitoring Instrument (OMI) and Microwave Limb Sounder (MLS) data (hereinafter referred to as OMI/MLS), have been investigated. We find that all four retrieved data sets show agreement within the error bars and exhibit strong seasonal variation, which differs in amplitude. The spatial distribution of tropospheric ozone observed shows pollution plumes related to the release of precursors at the different seasons in both hemispheres.

AMTD

6, 7811–7865, 2013

## Tropospheric ozone retrievals from SCIAMACHY observations

F. Ebojje et al.

Title Page

Abstract

Introduction

Conclusions

References

Tables

Figures

◀

▶

Back

Close

Full Screen / Esc

Printer-friendly Version

Interactive Discussion



# 1 Introduction

One important objective of SCIAMACHY, which flew as part of the payload of Envisat, was to investigate globally the chemical composition of the Earth's atmosphere (Burrows et al., 1995; Bovensmann et al., 1999; Gottwald and Bovensmann, 2011). It led to the development of the smaller nadir viewing GOME (Global Ozone Monitoring Experiment) (Burrows et al., 1999) and the first operational meteorological instrument GOME-2 (Callies et al., 2000; Munro et al., 2006) on the Metop series of platforms. These spectrometers fly in sun synchronous orbits in descending node and have equator crossing times between 09:30 and 10:30 LT in the morning. Retrieval of their ultra-violet or visible observations, yields important trace constituents: O<sub>3</sub>, nitrogen dioxide (NO<sub>2</sub>), sulphur dioxide (SO<sub>2</sub>), water vapour (H<sub>2</sub>O), chlorine dioxide (ClO<sub>2</sub>), bromine monoxide (BrO), iodine monoxide (IO), formaldehyde (HCHO), or glyoxal (CHO · CHO) on global scale (e.g., Burrows et al., 1999; Wagner et al., 2008).

SCIAMACHY employs three distinct viewing modes (nadir, limb, and occultation) during each orbit cycle to measure the sunlight transmitted and scattered by the Earth's atmosphere. The original concept of SCIAMACHY was based upon two spectrometers both capable of measuring in limb or nadir, resulting in simultaneous measurements. However, to reduce cost, the instrument was reduced to one spectrometer, which alternately observed in limb and nadir during an orbit.

The sampling was then optimized such that the limb profile and nadir observations are matched to observe the same air mass, facilitating a form of tomography (Fig. 1). This mode of observation was introduced to facilitate the separation of the tropospheric abundance of absorbing constituents from that in the middle atmosphere. The separation of tropospheric columns from the middle atmospheric columns of important atmospheric trace gases was one of the scientific goals for the SCIAMACHY project.

The vertical resolution of the retrieved trace gas profiles in the limb viewing mode of SCIAMACHY, when coupled with its nadir observations to yield the tropospheric column amount of a trace gas, provides added information as compared to the limited

AMTD

6, 7811–7865, 2013

## Tropospheric ozone retrievals from SCIAMACHY observations

F. Ebojje et al.

Title Page

Abstract

Introduction

Conclusions

References

Tables

Figures

◀

▶

Back

Close

Full Screen / Esc

Printer-friendly Version

Interactive Discussion

vertical resolution profiles retrieved from the observations of the nadir viewing ultra-violet spectrometers and the limited horizontal coverage of occultation experiments such as the HALogen Occultation Experiment (HALOE) (Russell III et al., 1993), Polar Ozone and Aerosol Measurement (POAM) (Lucke et al., 1999), and the Stratospheric

5 Aerosols and Gas Experiment (SAGE) (McCormick et al., 1989).

The limb-scatter technique for the retrieval of trace vertical profiles was first applied by the UltraViolet Spectrometer (UVS) on the Solar Mesosphere Explorer (SME) satellite to retrieve O<sub>3</sub> in the mesosphere (Rusch et al., 1984) and stratospheric NO<sub>2</sub> profiles (Mount et al., 1989). The Shuttle Ozone Limb Sounding Experiment/Limb Ozone

10 Retrieval Experiment (SOLSE/LORE) instrument demonstrated for the first time successfully the limb-scatter technique to derive stratospheric O<sub>3</sub> profiles (McPeters et al., 2000). The limb-scatter technique yields atmospheric information with enhanced sensitivity to a selection of trace constituents, good global coverage and relatively high vertical resolution (~3 km). The data products from the current generation of sensors  
15 suffer, dependent on the spatial resolution, from the high probability of cloud interference, horizontal resolution along the line of sight being large and complex viewing geometry, which requires highly complex spherical and multiple scattering radiation transfer modelling.

Satellite instruments utilizing nadir viewing geometry have a lower probability for  
20 cloud interference, good horizontal spatial resolution and vertical profiles of strongly absorbing species such as O<sub>3</sub> can be retrieved, but only with poor vertical resolution (7–10 km) (Hoogen et al., 1998, 1999; Meijer et al., 2006).

Global retrievals of tropospheric O<sub>3</sub> from satellite instruments are required to study its global distributions due to its relatively short lifetime and consequent variability. Important information on its spatial and temporal variability, sources and sinks, transport, and seasonal behavior can also be acquired from satellite instruments. However, the retrieval of tropospheric O<sub>3</sub> from space observations of the upwelling radiation at the top of the atmosphere requires accurate separation of stratospheric O<sub>3</sub>, which accounts on average for approximately 90 % of the total O<sub>3</sub> columns.

## Tropospheric ozone retrievals from SCIAMACHY observations

F. Ebojje et al.

[Title Page](#)

[Abstract](#)

[Introduction](#)

[Conclusions](#)

[References](#)

[Tables](#)

[Figures](#)

◀

▶

◀

▶

[Back](#)

[Close](#)

[Full Screen / Esc](#)

[Printer-friendly Version](#)

[Interactive Discussion](#)

A number of methods for retrieving tropospheric O<sub>3</sub> from satellite observations have been proposed, including methods using a residual approach, pioneered by Fishman and Larsen (1987). In this method the tropospheric O<sub>3</sub> columns were derived by subtracting the stratospheric O<sub>3</sub> columns from the total O<sub>3</sub> columns using a combination

5 of two different instruments. Different variants of this method have been developed over the years (e.g., Fishman et al., 1990; Fishman and Balok, 1999; Ladstätter-Weißenmayer et al., 2004; Thompson and Hudson, 1999; Ziemke et al., 1998, 2006, 2011; Schoeberl et al., 2007). Also, Kim et al. (2001) have used the scan angle geometry technique to retrieve tropical tropospheric O<sub>3</sub>, a method that requires multi-angle

10 measurements.

The direct retrieval of tropospheric O<sub>3</sub> from solar backscattered UV nadir spectra from satellite instruments such as GOME, OMI, SCIAMACHY etc., through the combination of forward model simulation, a priori knowledge and spectral fitting or using optimal estimation technique (Rodgers, 2000) has also been demonstrated (Munro et al., 15 1998; Hoogen et al., 1998, 1999; Liu et al., 2006, 2010, and references therein). However, the information content of the O<sub>3</sub> absorption in the nadir observation of the up-welling solar radiation is dominated by the stratospheric and mesospheric O<sub>3</sub> columns.

The approach of using penetration depth to provide vertical profiling was first proposed in the 1950s (Singer and Wentworth, 1957) and used for BUV and SBUV observations to retrieve O<sub>3</sub> vertical profile data products (Kramarova et al., 2013). The approach works well above the O<sub>3</sub> maximum in the stratosphere but does not provide much information about the vertical profile of O<sub>3</sub> below the O<sub>3</sub> maximum concentration in the stratosphere. Although the use in addition of knowledge of the topography, cloud tops, and the weak temperature dependence of the O<sub>3</sub> Huggins bands provides 20 additional information to help to separate tropospheric O<sub>3</sub> information, the required precision of measurements of the back scattered UV radiation is high to retrieve tropospheric O<sub>3</sub>. Making simultaneous measurements of the Hartley, Huggins, Chappuis, and Wulf bands of O<sub>3</sub> provides further information for use in the retrieval of O<sub>3</sub> vertical

## Tropospheric ozone retrievals from SCIAMACHY observations

F. Ebojje et al.

[Title Page](#)

[Abstract](#)

[Introduction](#)

[Conclusions](#)

[References](#)

[Tables](#)

[Figures](#)

◀

▶

[Back](#)

[Close](#)

[Full Screen / Esc](#)

[Printer-friendly Version](#)

[Interactive Discussion](#)

profiles. This is because the scattering in the lower atmosphere back to space is wavelength dependent in the ultraviolet-A (UV-A) and visible spectral regions.

However, the O<sub>3</sub> absorption features are weaker in the Huggins, Chappuis and Wulf bands. The signal to noise of the measurements of the upwelling radiance from the top of the atmosphere, which is determined by the size of the instrument optics and detector noise, then becomes critical as to whether this information can be separated from photon and detector noise and then be used, adding information or degrees of freedom to the retrieval of tropospheric O<sub>3</sub>.

In addition chlorophyll, liquid water and surface absorption features need to be very accurately accounted for in order to retrieve the total or tropospheric O<sub>3</sub> columns. Tropospheric O<sub>3</sub> has also been retrieved directly from nadir measurements of thermal infrared (TIR) emission (Aumann et al., 2003). However, as the signal in the thermal infrared depends on the thermal contrast, sensitivity is poor in the lower troposphere and maximizes in the upper troposphere and lower stratosphere. Another approach to retrieve information about tropospheric O<sub>3</sub> is to use the simultaneous observation of multiple UV, visible and TIR features, as first proposed in the GeoTROPE studies (Burrows et al., 2004). The TIR O<sub>3</sub> signal is dependent on the temperature profile, the O<sub>3</sub> profile and its amount. This technique has been implemented in the retrieval of vertical profiles of trace gases through the combination of infrared (IR) and UV nadir measurements as demonstrated by Bovensmann et al. (2004) and Cuesta et al. (2012) in the retrieval of tropospheric ozone using infrared radiance spectra recorded by the Infrared Atmospheric Sounding Interferometer (IASI) and GOME-2 ultraviolet measurements.

The retrieval of atmospheric trace gases using the residual approach by combining limb and nadir measurements from SCIAMACHY has been applied to O<sub>3</sub> and NO<sub>2</sub> (Sierk et al., 2006; Sioris et al., 2004; Beirle et al., 2010; Hilboll, 2013). The global retrieval of tropospheric O<sub>3</sub> from SCIAMACHY using the LNM technique is of great potential significance, as it is expected to characterize stratospheric inhomogeneity and provide an improved understanding of the monitoring of global tropospheric ozone. This

## Tropospheric ozone retrievals from SCIAMACHY observations

F. Ebojje et al.

[Title Page](#)

[Abstract](#)

[Introduction](#)

[Conclusions](#)

[References](#)

[Tables](#)

[Figures](#)

◀

▶

◀

▶

[Back](#)

[Close](#)

[Full Screen / Esc](#)

[Printer-friendly Version](#)

[Interactive Discussion](#)

data is needed to assess our understanding of the processes controlling tropospheric O<sub>3</sub> abundances and for testing chemical transport and chemistry climate models.

This manuscript provides the description of the SCIAMACHY LNM tropospheric O<sub>3</sub> retrieval, an error analysis, and describes a validation made by the comparison of tropospheric O<sub>3</sub> from SCIAMACHY with tropospheric O<sub>3</sub>, determined by using data from

5 ozonesondes and the O<sub>3</sub> data sets, retrieved from the measurements of other satellite instruments.

The subsequent sections of this manuscript are as follows: Sect. 2.1 briefly describes the SCIAMACHY instrument on Envisat and its applications relevant to this  
10 study, Sect. 3 summarizes the retrieval method used, Sect. 4 presents a sensitivity study, estimating both systematic and random errors from all relevant error sources. Section 5, which compares SCIAMACHY, TES, OMI/MLS, and ozonesondes observations, provides first validation results of the tropospheric O<sub>3</sub> columns retrieved from the SCIAMACHY limb-nadir matching technique, and Sect. 6 summarizes our principal  
15 findings and conclusions.

## 2 Instrument description

### 2.1 SCIAMACHY

SCIAMACHY (Burrows et al., 1995; Bovensmann et al., 1999), is a passive spectrometer, and part of the payload for ESA's Environmental Satellite (Envisat), launched into  
20 orbit on 28 February, 2002. Unfortunately, on 8 April, 2012 contact was lost with Envisat and thus far, ESA has failed to regain contact. Envisat orbited and will continue to orbit the earth in a sun-synchronous, near-polar orbit at a mean altitude of typically about 795 km with an inclination relative to the equatorial plane of 98.5°. It has an orbital period of about 100 min, thus completing about 14.3 orbits per day. Its local equator crossing time is 10:00 a.m. in descending node. SCIAMACHY measured the transmitted, reflected and scattered solar radiation in the ultraviolet (UV), visible,

AMTD

6, 7811–7865, 2013

## Tropospheric ozone retrievals from SCIAMACHY observations

F. Ebojje et al.

[Title Page](#)

[Abstract](#)

[Introduction](#)

[Conclusions](#)

[References](#)

[Tables](#)

[Figures](#)

◀

▶

◀

▶

[Back](#)

[Close](#)

[Full Screen / Esc](#)

[Printer-friendly Version](#)

[Interactive Discussion](#)



and near infrared (NIR) wavelength regions (214–2386 nm) with a spectral resolution varying between 0.22 nm and 1.48 nm. This is achieved with the aid of scan mirrors, which collect electromagnetic radiation and direct it to a telescope and then through the slit of the double monochrometer. The latter uses a prism to produce an intermediate spectrum, which is then separated into 8 channels, each comprising optics, a grating and diode array detector. The observations are contiguous from 214 to 1750 with two channels 1940–2040 nm and 2265–2380 nm.

The scan mirror system results in three different viewing geometries: limb, nadir and solar/lunar occultation observation geometries. In the nadir mode, the field of view of the instrument is oriented to the line-of-sight. This geometry allows the instrument to scan the region underneath the spacecraft by detecting upwelling solar radiation that has been scattered in the atmosphere and reflected by the Earth's surface. Also in this mode, the mirror scans across the satellite track and each full scan covers a ground area of approximately 30 km along track by 960 km across track with the footprint of a single observation being typically  $30 \times 60 \text{ km}^2$ . In the limb mode, the instrument line of sight is directed tangentially to the Earth surface. The instrument scans in the horizontal and vertical direction with elevation steps of approximately 3.3 km at the tangent point (Gottwald and Bovensmann, 2011). Due to the elevation steps performed by the instrument, the tangent point of the line-of-sight moves slightly towards the spacecraft as the satellite moves along the orbit. As the satellite moves around the Earth, the along-track extent of the limb pixels appear rather narrow (see for example the description in Gottwald and Bovensmann, 2011). The tangent height is raised in discrete steps from the surface up to about 100 or 150 km, thus permitting the retrieval of vertical absorber profiles by utilizing only scattered light. The instantaneous field of view at the tangent point is about 110 km (horizontally) by about 2.6 km (vertically). The ground scene of a SCIAMACHY limb scan is defined by the geolocation of the line-of-sight tangent point at the start and end of the state, which typically consists of about 31 horizontal scans with one complete limb scan taking about 60 s and for every limb state, four different vertical profiles are recorded. The horizontal across track coverage

## Tropospheric ozone retrievals from SCIAMACHY observations

F. Ebojje et al.

<a href="#">Title Page</a>	
<a href="#">Abstract</a>	<a href="#">Introduction</a>
<a href="#">Conclusions</a>	<a href="#">References</a>
<a href="#">Tables</a>	<a href="#">Figures</a>
<a href="#"></a>	<a href="#"></a>
<a href="#">Back</a>	<a href="#">Close</a>
<a href="#">Full Screen / Esc</a>	
<a href="#">Printer-friendly Version</a>	
<a href="#">Interactive Discussion</a>	

## 10 2.2 OMI/MLS and TES

OMI/MLS and TES are satellite instruments aboard the Aura spacecraft which was launched into a sun-synchronous polar orbit in July 2004 at an inclination angle of 98.2° and an altitude of 705 km. The spacecraft has an equatorial crossing time of approximately 01:45 p.m. in ascending node and takes about 98.8 min to cover an orbit thereby completing about 14.6 orbits per day.

TES is a Fourier transform IR spectrometer covering the spectral range of 650–3050 cm<sup>-1</sup> (3.3–15.4 μm) at a spectral resolution of 0.1 cm<sup>-1</sup> in the nadir viewing mode or 0.025 cm<sup>-1</sup> in the limb viewing mode (Beer, 2006). TES covers the globe in 16 days in the cross-track mode and in 3 days in the limb mode. For our analysis we used TES V003 ozone data downloaded from <http://eosweb.larc.nasa.gov/>, which were retrieved using optimal estimation technique (Rodgers, 2000) as described by Bowman et al. (2006). These data set have been validated with ozonesondes and aircraft data showing a bias of 3–10 ppbv (Boxe et al., 2009).

OMI is a UV-visible nadir viewing spectrometer detecting backscattered solar radiation over the 270–500 nm wavelength range with a spectral resolution of 0.42–0.63 nm (Leveld et al., 2006). It has a spatial resolution of 13 × 24 km<sup>2</sup> and covers the globe in one day, thus providing daily information on the total O<sub>3</sub> columns. Measurements of ozone from OMI were determined using the OMI-TOMS retrieval algorithms version

Title Page

Abstract

Introduction

Conclusions

References

Tables

Figures

◀

▶

◀

▶

Back

Close

Full Screen / Esc

Printer-friendly Version

Interactive Discussion



8.5 described in <http://eospso.gsfc.nasa.gov/sites/default/files/atbd/ATBD-OMI-02.pdf> (Ziemke et al., 2011).

The MLS instrument is a microwave limb sounder that measures vertical profiles of O<sub>3</sub>, providing information on the stratospheric O<sub>3</sub> column. Information on the MLS version 3.3 ozone measurements as well as data quality description document are available at <http://disc.sci.gsfc.nasa.gov/gesNews/>. An analysis of stratospheric ozone columns derived from MLS version 3.3 and an earlier version 2.2, which has been validated by Froidevaux et al. (2008), show a systematic offset of about 2.5 DU (Ziemke et al., 2011). The MLS measurements are made about 7 minutes before OMI views the same location during ascending (daytime) orbital tracks. The tropospheric O<sub>3</sub> columns are derived by subtracting the vertically integrated MLS O<sub>3</sub> profiles from the OMI total column O<sub>3</sub>. For our analysis we used OMI/MLS tropospheric ozone column downloaded from <http://acdb-ext.gsfc.nasa.gov/>.

### 2.3 Ozonesondes

An ozonesonde is a lightweight ozone measuring instrument carried aloft a small balloon. It comprises an electrochemical cell filled with a Potassium Iodide (KI) solution and a meteorological radiosonde (Komhyr, 1967). When ambient air is pumped through the cell, O<sub>3</sub> present in the air undergoes redox reactions with the KI solution (Eq. 1 and 2) and generates an electric current, which is considered to be proportional to the concentration of ozone in the sampled air after correcting for background effects.



The radiosonde also measures the ambient air temperature, pressure, relative humidity and transmits all the acquired information back to a ground receiving station during the balloon ascent before bursting at an altitude typically of around 35 km depending

Title Page

Abstract

Introduction

Conclusions

References

Tables

Figures

◀

▶

◀

▶

Back

Close

Full Screen / Esc

Printer-friendly Version

Interactive Discussion

## Tropospheric ozone retrievals from SCIAMACHY observations

F. Ebojje et al.

<a href="#">Title Page</a>	
<a href="#">Abstract</a>	<a href="#">Introduction</a>
<a href="#">Conclusions</a>	<a href="#">References</a>
<a href="#">Tables</a>	<a href="#">Figures</a>
<a href="#">◀</a>	<a href="#">▶</a>
<a href="#">Back</a>	<a href="#">Close</a>
<a href="#">Full Screen / Esc</a>	

[Printer-friendly Version](#)

[Interactive Discussion](#)

on the state of the atmosphere. The types of ozonesonde used in our validation include the electrochemical concentration cell (ECC) (Komhyr, 1969, 1971), Brewer-Mast (BM) (Brewer and Milford, 1960), and the carbon iodine cell (KC96) (Kobayashi and Toyama, 1966).

- These different types of ozonesondes operate on the same principle, as discussed above, but differ in instrumental layout and design (Smit, 2002). The ozonesondes data used in our analysis were obtained from <http://www.woudc.org/> and <http://croc.gsfc.nasa.gov/shadow/> (Thompson et al., 2003). From these datasets, we first determined the tropopause heights from the temperature profile measurements by using the thermal tropopause definition before deriving the tropospheric O<sub>3</sub> column (TOC) by integrating the concentration ( $c_i$ ) from the surface to the tropopause as given by the expression,

$$\text{TOC} = \frac{1}{2} \sum_{i=1}^{i_{\max}} [(c_{i+1} + c_i)(h_{i+1} - h_i)] \quad (3)$$

and  $c_i$  is given by

$$c_i = \frac{N_A P_i}{R T_i}, \quad (4)$$

- where  $i$  represents the level index,  $h$  is the height,  $N_A$  is Avogadro's number,  $R$  is the ideal gas constant, and  $T$  and  $P$  are the temperature and O<sub>3</sub> partial pressure, respectively. The ozonesondes provide ozone partial pressure on a vertical scale of atmospheric pressure with a vertical resolution of ~150 m at an accuracy of 5–10 % in the troposphere (WMO, 1999; Smit et al., 2007)

### 3 Method and Data analysis from SCIAMACHY

#### 3.1 Stratospheric ozone profile retrievals from SCIAMACHY limb measurements

Stratospheric O<sub>3</sub> profiles are retrieved from SCIAMACHY limb-viewing measurements.

- 5 The method employed for the retrieval of version 2.9 used in this analysis is an update of version 2.1 described in Sonkaew et al. (2009), which involves employing the surface albedo database by Matthews (1984) in the forward radiative transfer calculations, and using the empirical aerosol extinction profile model ECSTRA originally developed by Fussen and Bingen (1999). Briefly, the retrieval of stratospheric O<sub>3</sub> profiles utilizes the combination of three wavelengths (525, 600 and 675 nm) in the O<sub>3</sub> Chappius band (Flittner et al., 2000; von Savigny et al., 2003) and several wavelengths in the UV Hartley-Huggins band (264, 267.5, 273.5, 283, 286, 288, 290 and 305 nm) to cover the altitude range from 10 to 80 km. In the selection of the wavelengths in the Hartley-Huggins bands, care is taken to avoid contamination of the limb scattering measurements by airglow emissions and strong Fraunhofer lines (Rohen, 2006). The inversion of the measurement vector is performed using a non-linear Optimal Estimation iteration scheme together with the SCIATRAN radiative transfer model (RTM) (Rozanov et al., 2005). As in satellite measurements, there exist errors in the retrieval of the stratospheric ozone profiles, which were potentially found to arise from clouds, 15 tangent height registration, effective albedo, and aerosol extinction. External stray light, which is referred to as the contamination from outside the field of view of the instrument, e.g. from clouds and the earth brightness, is another source of error. To reduce the effect of clouds and albedo on the retrieval, the radiance profiles are normalized by the limb radiance at upper tangent heights which vary depending on wavelength.
- 20

AMTD

6, 7811–7865, 2013

#### Tropospheric ozone retrievals from SCIAMACHY observations

F. Ebojje et al.

[Title Page](#)

[Abstract](#)

[Introduction](#)

[Conclusions](#)

[References](#)

[Tables](#)

[Figures](#)

◀

▶

[Back](#)

[Close](#)

[Full Screen / Esc](#)

[Printer-friendly Version](#)

[Interactive Discussion](#)



### 3.2 Total ozone column retrievals from SCIAMACHY nadir measurements

The Weighting Function Differential Optical Absorption Spectroscopy (WFDOAS) algorithm (Coldewey-Egbers et al., 2005; Weber et al., 2005) is used to retrieve total O<sub>3</sub> columns from the SCIAMACHY nadir-viewing measurements. This technique fits the vertically integrated O<sub>3</sub> weighting function instead of the O<sub>3</sub> cross-section like in the standard DOAS retrieval to the sun-normalized radiances in order to directly retrieve the vertical column amounts. The fitting window of 326.6–334.5 nm is used for the total O<sub>3</sub> column retrieval. To obtain the weighting function for the change in the total O<sub>3</sub> column, the weighting function calculated at each altitude using the GOMETRAN radiation transfer code (Rozanov et al., 1998) are integrated vertically. This approach suits well the retrievals of strong absorbers like O<sub>3</sub> in the UV. The WFDOAS technique accounts for the effect of rotational Raman scattering (Ring effect) by using a precalculated data base of Raman reference spectra which is tabulated as a function of O<sub>3</sub> column density, solar zenith angle, surface albedo, and altitude (Coldewey-Egbers et al., 2005). The validation of the total O<sub>3</sub> column with ground based measurements from the WOUDC (World Ozone and UV Radiation Data Centre) shows good agreement to within ±2 % with small seasonal differences (Bracher et al., 2005; Weber et al., 2007). In the polar regions, and at very high solar zenith angles, biases can be larger (Weber et al., 2005).

### 20 3.3 Combination of SCIAMACHY limb and nadir measurements

The SCIAMACHY LNM observations have the objective of yielding accurate retrievals of the tropospheric amount of trace species, which have significant stratospheric absorption. The SCIAMACHY instrument is designed such that it alternates between limb and nadir geometries so that the region probed during the limb scan can be observed 25 7 min later during the nadir scan. This technique yields the vertical stratospheric concentration profiles of the trace gas directly over the region of the nadir measurements of total columns. Integrating the coincident stratospheric profiles from the tropopause

AMTD

6, 7811–7865, 2013

## Tropospheric ozone retrievals from SCIAMACHY observations

F. Ebojje et al.

Title Page

Abstract

Introduction

Conclusions

References

Tables

Figures

◀

▶

Back

Close

Full Screen / Esc

Printer-friendly Version

Interactive Discussion



upwards determines the stratospheric vertical column density above the target area (see Eq. 5). The subtraction of the resulting stratospheric column amount from the total column measured in nadir yields the tropospheric column amounts. Combining limb and nadir measurements from the same instrument like in the case of SCIAMACHY

- 5 (Sierk et al., 2006; Beirle et al., 2010) assumes that the column of O<sub>3</sub> above the nadir state is proportional to the tropospheric O<sub>3</sub> column. This in a way should be associated with lower uncertainties than those approaches that require different instruments that do not allow exact matches of air masses in space and time.

To implement the LNM technique, we computed the tropopause heights from the operational meteorological model data provided by the European Center for Medium Range Weather Forecasts (ECMWF). These data comprise three-dimensional fields of pressure, temperature, and wind vectors on a latitude/longitude grid of 1.5° resolution with 91 levels and 4 analysis times daily. From these data, the location of the tropopause is obtained by applying the dynamical (potential vorticity) and the thermal (lapse rate) definitions of the tropopause. The thermal tropopause, which assumes that the stratosphere is more stably stratified than the troposphere, is defined as the lowest level at which the lapse rate is 2 K km<sup>-1</sup> or less, provided also that the average lapse rate between this level and all higher levels within 2 km does not exceed 2 K km<sup>-1</sup> (WMO, 1957). To determine the tropopause height using both criteria we followed an approach similar to that discussed in Hoinka (1998). The combination of the dynamical and thermal criteria enabled a clear definition of the boundary between the troposphere and the stratosphere at all latitudes. For the tropics (i.e. ±20° latitude from the equator) we applied the thermal criterion and from the mid-latitudes to the poles (latitudes higher than 30° in both hemispheres) we applied the dynamical criterion. In the transition region between the two regimes (20°–30° in both hemispheres) both criteria were used and weighted with the distance from the regime boundaries. The ECMWF analysis data are produced every six hours and the value closest in time to the SCIAMACHY observation is used. The tropopause heights determined show variation on a daily basis (Fig. 2) and have been validated with tropopause heights determined

## Tropospheric ozone retrievals from SCIAMACHY observations

F. Ebojje et al.

[Title Page](#)

[Abstract](#)

[Introduction](#)

[Conclusions](#)

[References](#)

[Tables](#)

[Figures](#)

◀

▶

[Back](#)

[Close](#)

[Full Screen / Esc](#)

[Printer-friendly Version](#)

[Interactive Discussion](#)

from radiosondes flying along with ozonesondes. The comparisons of the tropopause heights generated from ozonesondes and ECMWF show good agreement with a mean difference of less than 500 m for the stations considered in both hemispheres. The tropospheric O<sub>3</sub> columns from SCIAMACHY were derived by first integrating the stratospheric and mesospheric O<sub>3</sub> profiles from the height of the tropopause to about 80 km and the resulting stratospheric and mesospheric O<sub>3</sub> columns (see Eq. 5) were subtracted from the total O<sub>3</sub> columns.

$$C = \sum_{i=80}^{i=80} \left( \frac{N(z_{i-1}) + N(z_i)}{2} \right) (z_i - z_{i-1}), \quad (5)$$

where  $C$  is the integrated stratospheric ozone profile above the tropopause height (tph), which is referred to as the stratospheric ozone column,  $N_{(z)}$  is the stratospheric ozone profile in number density,  $z$  is the altitude and  $i$  is the index. At the higher latitudes where the tropopause is below 10 km, the stratospheric O<sub>3</sub> profiles below the retrieval grid were constructed from an ozonesonde climatological profiles (2003–2011) scaled to match the lower part of the retrieved SCIAMACHY profile. Since the air mass covered by a single limb measurement is about 400 km (along track)  $\times$  240 km (across track) and correspondingly averaged nadir state covers 30 km (across track)  $\times$  60 km (along track), in a clear sky condition and under the assumption of the homogeneity of stratospheric ozone, a single tropospheric column is estimated to cover a ground area of about 60 km  $\times$  240 km. As the limb observations are greatly affected by clouds we only used cloud free pixels and for nadir observations, pixels with cloud fraction of less than 0.1 were considered in the retrievals (see Sect. 4). Furthermore, to minimize uncertainties in our retrieved tropospheric O<sub>3</sub>, we considered measurements from the descending part of the orbit with solar zenith angles less than 80°, because of the decrease in tropospheric sensitivity to O<sub>3</sub> at higher solar zenith angles.

## Tropospheric ozone retrievals from SCIAMACHY observations

F. Ebojje et al.

[Title Page](#)

[Abstract](#)

[Introduction](#)

[Conclusions](#)

[References](#)

[Tables](#)

[Figures](#)

◀

▶

[Back](#)

[Close](#)

[Full Screen / Esc](#)

[Printer-friendly Version](#)

[Interactive Discussion](#)

## 4 Error analysis

This section presents a summary of the contribution of the various error sources to the overall error in the retrieved tropospheric O<sub>3</sub> columns as well as the derived global error budget. Table 1 gives an overview of the error sources in the tropospheric O<sub>3</sub> retrieval 5 using the SCIAMACHY limb-nadir-matching technique. Clouds play an important role in reflection, absorption and transmission of solar radiation, thus affecting trace gas retrievals. In the nadir measurements for example, clouds have three major effects on the O<sub>3</sub> retrievals. These comprise the albedo effect, the increase in-cloud absorption, and a shielding effect (Koelemeijer and Stammes, 1999; Newchurch et al., 2001). The 10 albedo and shielding effect lead to apparent increase of the depth of absorption bands of O<sub>3</sub> and thus an underestimation of the total O<sub>3</sub> columns. Also, the shielding effect leads to the underestimation of the vertical O<sub>3</sub> column densities.

In our analysis we employed two different cloud algorithms, one based on nadir observations and the other based on limb observations. For the case of the total O<sub>3</sub> 15 columns we used the SemiAnalytical CloUd Retrieval Algorithm (SACURA), which determines the cloud fraction, cloud-top-height, and other cloud parameters from the oxygen A-band (760 nm) (Kokhanovsky and Rozanov, 2004). SACURA accounts for the penetration of radiation in the clouds using analytical expressions. In the total O<sub>3</sub> columns retrieval using the WFDOAS techniques, clouds are treated as Lambertian 20 reflecting surfaces (Coldewey-Egbers et al., 2005; Weber et al., 2005). Clouds are also detected in the limb viewing mode and are accounted for by using the SCIAMACHY Cloud Detection Algorithm (SCODA) for limb radiance measurements (Eichmann et al., 2009).

SCODA uses the colour index ratios in the vertical radiance profiles at different wavelength pairs in the visible and near infrared to determine cloud top height and cloud 25 thermodynamic phase. As mentioned above, since tropospheric O<sub>3</sub> columns constitute only about 10 % of the total O<sub>3</sub> columns, small errors associated with clouds might significantly affect the derived tropospheric O<sub>3</sub> columns. Therefore, for proper

Title Page

Abstract

Introduction

Conclusions

References

Tables

Figures

◀

▶

Back

Close

Full Screen / Esc

Printer-friendly Version

Interactive Discussion

retrieval of tropospheric O<sub>3</sub> columns, limb scenes that are contaminated with clouds were screened out while total O<sub>3</sub> columns data that have a cloud fraction of less than 0.1 were used. A sensitivity analysis showed that an increase in cloud fraction threshold by 10 % on average reduces SCIAMACHY tropospheric ozone by about 1 DU.

The other potential sources of errors are from the stratospheric O<sub>3</sub> columns, total O<sub>3</sub> columns, and the computation of the tropopause height. Among these other error sources, the stratospheric O<sub>3</sub> columns contribute most to the total errors (see Table 1). The error contribution from the stratospheric O<sub>3</sub> columns (soc) which originated from the retrieval of stratospheric O<sub>3</sub> profiles (see Sect. 3.1) was computed from errors resulting from uncertainties in the assumed surface albedo (ab), aerosol extinction profile (ae), ozone absorption cross section (ac), pressure profile (pr), tangent height information (th), temperature profiles (temp) and the signal-to-noise ratio (snr) of the radiance measurements (see Tables 2 and 3).

The contributions from each of the different parameter errors on the retrieved O<sub>3</sub> profiles were computed using the SCIATRAN retrieval model on stratospheric ozone profiles in both hemispheres at different solar zenith angles. To achieve this, the simulated O<sub>3</sub> profiles for a given reference parameter were compared with the ozone profiles based on an altered value of the same parameter that lies within the range of the error. For example, to compute the impact of albedo on the retrieved O<sub>3</sub> profile, the ozone profile with constant albedo value of 0.3 was taken as a reference and compared the ozone profiles retrieved from different forward model simulations.

In other words, to account for instance, for an albedo error of  $\pm 0.1$ , O<sub>3</sub> profiles with albedo values of 0.2 and 0.4 were compared with O<sub>3</sub> profiles with albedo value of 0.3. A similar approach was carried out for the other error parameters and the deviation of the O<sub>3</sub> profile for a given parameter value from the reference value is defined as the parameter error (Rahpoe et al., 2013). The most influential errors among the different parameters used in the stratospheric O<sub>3</sub> profile retrieval are aerosol and tangent height registration (Tables 2 and 3). To quantify the effects of these parameter errors on stratospheric O<sub>3</sub> profile retrievals, we combined the different parameter errors using

## Tropospheric ozone retrievals from SCIAMACHY observations

F. Ebojie et al.

[Title Page](#)

[Abstract](#)

[Introduction](#)

[Conclusions](#)

[References](#)

[Tables](#)

[Figures](#)

◀

▶

[Back](#)

[Close](#)

[Full Screen / Esc](#)

[Printer-friendly Version](#)

[Interactive Discussion](#)

Gaussian error propagation in a simplified form as shown in Eq. (6).

$$\begin{aligned}\sigma_{\text{sco}}^2 \approx & \sigma_{\text{ab}}^2 \left( \frac{\partial(\text{sco})}{\partial(\text{ab})} \right)^2 + \sigma_{\text{ae}}^2 \left( \frac{\partial(\text{sco})}{\partial(\text{ae})} \right)^2 + \sigma_{\text{ac}}^2 \left( \frac{\partial(\text{sco})}{\partial(\text{ac})} \right)^2 \\ & + \sigma_{\text{pr}}^2 \left( \frac{\partial(\text{sco})}{\partial(\text{pr})} \right)^2 + \sigma_{\text{snr}}^2 \left( \frac{\partial(\text{sco})}{\partial(\text{snr})} \right)^2 \\ & + \sigma_{\text{th}}^2 \left( \frac{\partial(\text{sco})}{\partial(\text{th})} \right)^2 + \sigma_{\text{temp}}^2 \left( \frac{\partial(\text{sco})}{\partial(\text{temp})} \right)^2\end{aligned}\quad (6)$$

Similarly, the errors from the different error sources in the retrieval of total O<sub>3</sub> columns (Coldewey-Egbers et al., 2005) were combined using Gaussian error propagation. In

- 5 the case of the total O<sub>3</sub> column retrieval, the largest contribution to the error sources is identified to come from the a-priori errors associated with the O<sub>3</sub> climatology and assumptions in the derived effective parameters (Coldewey-Egbers et al., 2005). The extensive validation carried out by Weber et al. (2005), shows that the monthly mean error in the total column ozone is about 1 %. The error in tropospheric O<sub>3</sub> columns  
10 associated with errors in the tropopause height was accounted for by integrating the shift in altitude using trapezoidal rule. Figures 3 and 4 show the monthly averaged tropospheric O<sub>3</sub> column errors together with the error contributions from the stratospheric O<sub>3</sub> columns, the total O<sub>3</sub> columns as well as the errors in the tropopause height for January and July 2003, respectively. January 2003 shows a bump in the error contribution  
15 from the stratospheric O<sub>3</sub> columns between 40° N and 50° N with a maximum value of ~ 5.5 DU near 50° N. In the Southern Hemisphere the error contribution from the stratospheric O<sub>3</sub> columns increase from about 3.5 DU at 30° S to 7.5 DU at 65° S where it remains constant up to about 85° S. A similar bump, although with a lower amplitude is also observed in the Northern Hemisphere from the total O<sub>3</sub> columns for the same month. The effect of the tropopause heights is also seen to exhibit some zonal variability as a result of the variation in tropospheric ozone. These features, which could be due to changes in stratospheric temperature are clearly observable in the tropospheric O<sub>3</sub> column errors, where a mean error contribution of 5.5 DU, which is about  
20

AMTD

6, 7811–7865, 2013

## Tropospheric ozone retrievals from SCIAMACHY observations

F. Ebojje et al.

[Title Page](#)

[Abstract](#)

[Introduction](#)

[Conclusions](#)

[References](#)

[Tables](#)

[Figures](#)

◀

▶

[Back](#)

[Close](#)

[Full Screen / Esc](#)

[Printer-friendly Version](#)

[Interactive Discussion](#)



20 % error in the mean tropospheric ozone columns is recorded in January 2003. In July 2003, there is no observable sharp increase of errors in the Northern Hemisphere as observed in January 2003, but similar features as in January 2003 are depicted in the Southern Hemisphere (Fig. 4). The effects of tropopause height in both months are low, accounting for less than 0.1 DU of the error in tropospheric ozone retrieval.

In general, there is not much variation in the monthly average error contribution from the different error sources as shown in Table 1. The annual average error contribution from the stratospheric O<sub>3</sub> columns is about 4.6 DU, accounting for ~1.8 % error in mean stratospheric ozone columns. The mean error in the total column for 2003 is less than 3 DU, which is 1 % of the error in mean total ozone columns. The ozone error caused by tropopause height error in 2003 is less than 0.1 DU, accountng for ~1 % of the error in mean tropospheric O<sub>3</sub> column as a result of the effect of the height of the tropopause. The effect of these different error sources become larger in the retrieved tropospheric ozone columns accounting for a mean error of about 5.6 DU, which results to about 18 % error in the annual mean of the tropospheric O<sub>3</sub> columns.

## 5 Validation and intercomparisons of SCIAMACHY tropospheric ozone

### 5.1 Intercomparison of Tropospheric ozone columns from SCIAMACHY, TES, OMI/MLS and ozonesondes

The error of our retrieved tropospheric O<sub>3</sub> from SCIAMACHY was investigated by comparing the tropospheric O<sub>3</sub> columns from SCIAMACHY with the tropospheric O<sub>3</sub> columns measured by balloon-borne ozonesondes, and those retrieved from TES and the combined OMI/MLS data products (Table 4). Time series plots of ozonesondes and collocated, SCIAMACHY, TES and OMI/MLS measurements were produced so as to compare tropospheric O<sub>3</sub> values from SCIAMACHY with both in-situ measurements and those of other satellite instruments. Comparisons with ozonesondes pose some challenges as their measurements correspond to advected measurements along tra-

[Title Page](#)[Abstract](#)[Introduction](#)[Conclusions](#)[References](#)[Tables](#)[Figures](#)[◀](#)[▶](#)[Back](#)[Close](#)[Full Screen / Esc](#)[Printer-friendly Version](#)[Interactive Discussion](#)

## Tropospheric ozone retrievals from SCIAMACHY observations

F. Ebojie et al.

[Title Page](#)

[Abstract](#)

[Introduction](#)

[Conclusions](#)

[References](#)

[Tables](#)

[Figures](#)

◀

▶

◀

▶

[Back](#)

[Close](#)

[Full Screen / Esc](#)

[Printer-friendly Version](#)

[Interactive Discussion](#)

## Tropospheric ozone retrievals from SCIAMACHY observations

F. Ebojie et al.

[Title Page](#)

[Abstract](#)

[Introduction](#)

[Conclusions](#)

[References](#)

[Tables](#)

[Figures](#)

◀

▶

◀

▶

[Back](#)

[Close](#)

[Full Screen / Esc](#)

[Printer-friendly Version](#)

[Interactive Discussion](#)

**Tropospheric ozone retrievals from SCIAMACHY observations**

F. Ebojie et al.

[Title Page](#)[Abstract](#)[Introduction](#)[Conclusions](#)[References](#)[Tables](#)[Figures](#)[◀](#)[▶](#)[◀](#)[▶](#)[Close](#)[Full Screen / Esc](#)[Printer-friendly Version](#)[Interactive Discussion](#)

45 DU over the entire time series. Over this station, TES and ozonesonde records an averaged peak value of above 40 DU during the northern summer months.

The intercomparisons plots of SCIAMACHY tropospheric ozone values with other three satellite measurements over ozonesonde stations in the Southern Hemisphere, including Java ( $7.50^{\circ}$  S,  $112.60^{\circ}$  E) (Fig. 10), and Samoa ( $14.23^{\circ}$  S,  $170.56^{\circ}$  W) (Fig. 11), Broadmeadows ( $37.68^{\circ}$  S,  $144.95^{\circ}$  E) (Fig. 12), and Macquarie Island ( $54.50^{\circ}$  S,  $158.95^{\circ}$  E) (Fig. 13), also show good agreement in their seasonal variations. For instance, over JAVA, the tropospheric ozone values from all the instruments follow a similar pattern but there exist some peak ozone values observed by ozonesondes which are not captured by the satellite instruments. The seasonal behaviour of the tropospheric ozone retrieved from SCIAMACHY over Samoa, Broadmeadows and Macquarie Island follows a similar pattern with the values derived from the other instruments, though SCIAMACHY values appear shifted to the right over Macquarie Island. The relative difference for all stations considered shows that SCIAMACHY tropospheric ozone values over the entire data sets has good agreement with ozonesondes with a value of 0.06, while the relative difference of TES and OMI/MLS to ozonesondes are 0.11 and  $-0.10$ , respectively. In summary, all the instruments show a similar pattern over the ozonesonde stations reflecting the effect of the transport of precursors on tropospheric ozone production. SCIAMACHY, TES and OMI/MLS 0.06, 0.11,  $-0.10$ .

## 5.2 Global distribution and comparison of Tropospheric ozone columns from SCIAMACHY, TES and OMI/MLS

Global measurements of tropospheric  $O_3$  are needed to test our understanding of its sources and sinks. They provide continuous temporal and spatial observation, which are useful for the identification of sources, seasonal variations, and long-range transport of air pollutants (Creilson et al., 2003, 2005). They also provide observations, which allow for the generation of temporally extended records that are vital for the investigation of long term trend (Kim and Newchurch, 1996; Fishman et al., 2005; Valks et al., 2008). Tropospheric  $O_3$  is a strongly seasonal pollutant exhibiting usually

higher concentrations in the warm summer months. The tropospheric O<sub>3</sub> seasonality is caused by variation in tropospheric background O<sub>3</sub>, temporal variation of precursor emissions (NO<sub>x</sub>, VOCs, CO, CO<sub>2</sub>, CH<sub>4</sub>), systematic seasonal shifts of transport meteorology as well as by the seasonality of photochemical oxidation and removal processes.

For example, Fig. 14 shows the global distributions of tropospheric O<sub>3</sub> for four seasons, winter (December-January-February (DJF)), summer (June-July-August (JJA)) spring (March-April-May (MAM)) and autumn (September-October-November (SON)) in 2003. Significant differences between the northern and Southern Hemispheres as well as differences between the seasons are well represented in the plots. The seasonal distribution of tropospheric O<sub>3</sub> in both hemispheres shows good correlation with its precursors (Logan and Kirchhoff, 1986; Liu et al., 2008). For instance, in the Southern Hemisphere there is good correlation with the seasonal variation of biomass burning in Africa and South America during the northern winter months, which is mostly pronounced in northern autumn (Kim and Newchurch , 1998). Also observed is the correlation with photochemical production of O<sub>3</sub>, resulting from anthropogenic effects due to NO<sub>x</sub> and hydrocarbon emission in the northern summer (Lawrence and Crutzen, 1999; Ran et al., 2012). During northern spring, the low O<sub>3</sub> values over the tropical eastern pacific, which is attributed to the increase in HO<sub>x</sub> concentration (Liu et al., 2005), is captured by SCIAMACHY.

To further investigate the tropospheric O<sub>3</sub> columns retrieved from SCIAMACHY, we compared our results with those from TES and OMI/MLS, which were overlaid with tropospheric O<sub>3</sub> values from ozonesondes (filled circles). In the seasonal plots shown in Fig. 15, similar features as well as variability in regional patterns can be observed for all satellite datasets. These variations could result from the differences in operation of the instruments and algorithms used in the retrieval. All three instruments have different vertical resolutions and overpass times, the cloud detection and removal algorithm may also be different for the different instruments. For example, in the JJA panel of Fig. 15, OMI/MLS, TES and SCIAMACHY captured plumes of high tropospheric O<sub>3</sub> columns of about 35–50 DU over eastern region of United States, regions of eastern

Title Page

Abstract

Introduction

Conclusions

References

Tables

Figures

◀

▶

Back

Close

Full Screen / Esc

Printer-friendly Version

Interactive Discussion

Asia, Northern Atlantic and Northern Pacific, although the tropospheric ozone values from TES is slightly higher than that of SCIAMACHY and OMI/ MLS. These high tropospheric ozone values from TES are slightly more pronounced over the Mediterranean and Southern Europe, reaching a value of above 55 DU, as compared to the tropo-

- 5 spherical ozone values from the other satellite instruments. The tropospheric ozone values from the ozonesonde instruments in these region also show corresponding high values as observed by TES, although slightly lower. Also during the JJA season, the distributions of tropospheric ozone from SCIAMACHY and OMI/MLS have a similar pattern over the region of Africa and in the Southern Hemisphere. Pollution plumes, which
- 10 appear to be emanating from the coast of West Africa and traveling towards the Southern Atlantic, Madagascar, and across the Indian ocean and Australia are observed by all three instruments, although the values observed by SCIAMACHY and OMI/MLS are lower than those of ozonesondes and TES. Low tropospheric  $O_3$  is found in the tropical regions of Western Pacific, Thailand, Cambodia, Indian Ocean, and East Africa by
- 15 SCIAMACHY and OMI/MLS instruments during the boreal summer.

- In the northern hemisphere autumn, SCIAMACHY and TES show similar pollution plumes in both hemispheres, which are close in agreement with the values recorded by the ozonesonde instruments. But the tropospheric ozone values from OMI/MLS are low in both hemisphere. For example, the broad ozone maximum observed over the
- 20 Southern Atlantic, the coast of South Africa and Madagascar, transport along the Indian ocean towards Australia and plumes emanating from eastern Australia (Fishman et al., 2003) are captured by all three instruments with OMI/MLS tropospheric  $O_3$  columns being lower than TES and SCIAMACHY values. Higher values of  $O_3$  are also seen by all three satellite instruments downwind of the United States, North Atlantic, Europe and
- 25 Asia. SCIAMACHY values over Southern Europe and the middle east are similar to the values observed by TES and ozonesondes. Also, observed from all three instruments during the SON season is the plume over the Pacific, although OMI/MLS tropospheric  $O_3$  values are lower than SCIAMACHY, ozonesondes, and TES tropospheric  $O_3$  values over these regions. Another interesting feature are the low tropospheric  $O_3$  columns

## Tropospheric ozone retrievals from SCIAMACHY observations

F. Ebojie et al.

<a href="#">Title Page</a>	
<a href="#">Abstract</a>	<a href="#">Introduction</a>
<a href="#">Conclusions</a>	<a href="#">References</a>
<a href="#">Tables</a>	<a href="#">Figures</a>
<a href="#"></a>	<a href="#"></a>
<a href="#">Back</a>	<a href="#">Close</a>
<a href="#">Full Screen / Esc</a>	
<a href="#">Printer-friendly Version</a>	
<a href="#">Interactive Discussion</a>	

## Tropospheric ozone retrievals from SCIAMACHY observations

F. Ebojie et al.

[Title Page](#)

[Abstract](#)

[Introduction](#)

[Conclusions](#)

[References](#)

[Tables](#)

[Figures](#)

◀

▶

◀

▶

[Back](#)

[Close](#)

[Full Screen / Esc](#)

[Printer-friendly Version](#)

[Interactive Discussion](#)



over the Sahara Desert (Fishman et al., 2003) and South America at the location of the Andes Mountains, which are depicted in the seasonal plots from SCIAMACHY and OMI/MLS. This feature is highly pronounced during boreal spring and summer.

In the northern spring, the distribution of tropospheric ozone from SCIAMACHY in the Northern Hemisphere follows a similar pattern with that of the distribution from TES. These similar features are well observed in the enhanced pollution features downwind of south east Asia and towards the Northern Pacific with the tropospheric ozone values from the two satellite instruments in close agreement with the regional values from the ozonesonde instruments. The low ozone values over the inland region of South America and South Africa as depicted by both SCIAMACHY and OMI/MLS are not well captured by TES. The ozonesonde tropospheric ozone values over the inland region of South America agree better than the values recorded by the other satellite instruments. TES tropospheric ozone values agree better with the values from ozonesonde instruments over South Africa and towards Australia than the values from SCIAMACHY and OMI/MLS. Although some similar features can be observed from the tropospheric ozone distribution from SCIAMACHY, TES and OMI/MLS, the values of OMI/MLS are lower as observed over the Northern Pacific, Eastern region of America, and Europe. A plume of elevated  $O_3$  observed by the three satellite instruments across the Northern Atlantic, the Eastern region of America, Europe, central China, the Mediterranean, North Africa, Eastern Asia and over west central Africa could be due to biomass burning. Also, during northern spring SCIAMACHY tropospheric  $O_3$  column over South America and along the southern Atlantic, Indian ocean, and over Australia is closer to the tropospheric  $O_3$  values from OMI/MLS than TES. The very low values over the Andes and tropical Western Pacific as observed by SCIAMACHY and OMI/MLS are well defined during this season.

During northern winter months, tropospheric  $O_3$  values of about 32–36 DU observed over the North Pacific, the coast of the United States and Atlantic are captured by SCIAMACHY and TES but OMI/MLS values are lower, about 18–25 DU in these regions. Unfortunately, there are no ozonesonde station in the Northern Pacific to compare

with. The higher pollution plumes over India and Eastern Asia, as observed by TES and SCIAMACHY, are not well captured by OMI/MLS. The pollution features over the Mediterranean observed by SCIAMACHY and TES are similar but SCIAMACHY tropospheric O<sub>3</sub> over Southern Europe during the DJF season is slightly higher than TES.

- 5 All three instruments also observed downwind pollution plume over Southern Atlantic and toward Australia during northern winter months.

## 6 Summary and conclusions

We have presented the the derivation of a new data product for tropospheric O<sub>3</sub> columns retrieved using limb-nadir matching observations made by SCIAMACHY from

- 10 2003 to 2011. The spatial resolution of the tropospheric O<sub>3</sub> data product, which was determined by the collocated limb and nadir resolution is taken to be 60 km (along track) × 240 m (across track) and the monthly mean values have errors estimated to be less than 6 DU which corresponds to about 17 % of the tropospheric ozone columns.

The study provides a comprehensive error budget, comprising the different error contributions to the retrieved tropospheric O<sub>3</sub> columns. The most important contributing factor to the error budget is the error on the stratospheric O<sub>3</sub> columns, which is estimated to be less than 5DU or 1.8 % globally. The other error sources are uncertainties in the total columns and the effect of the tropopause height on the tropospheric O<sub>3</sub> columns. Cloud interference which is supposed to be the major error source was accounted for by considering only limb O<sub>3</sub> profiles that are completely free of cloud contamination. In nadir geometry, we applied a cloud fraction threshold of 10 %. This is another source of bias to the retrieved tropospheric O<sub>3</sub> columns. The data set has been validated by comparison with the tropospheric ozone column determined from ozonesondes. Time series plots with other satellite instruments were also generated.

20 In the global plots for different seasons in 2003, SCIAMACHY tropospheric O<sub>3</sub> columns provide detailed information from which we were able to identify enhanced pollution events and transport. Comparison with tropospheric O<sub>3</sub> columns retrieved from TES

AMTD

6, 7811–7865, 2013

## Tropospheric ozone retrievals from SCIAMACHY observations

F. Ebojje et al.

Title Page

Abstract

Introduction

Conclusions

References

Tables

Figures

◀

▶

Back

Close

Full Screen / Esc

Printer-friendly Version

Interactive Discussion



## Tropospheric ozone retrievals from SCIAMACHY observations

F. Ebojje et al.

[Title Page](#)

[Abstract](#)

[Introduction](#)

[Conclusions](#)

[References](#)

[Tables](#)

[Figures](#)

◀

▶

[Back](#)

[Close](#)

[Full Screen / Esc](#)

[Printer-friendly Version](#)

[Interactive Discussion](#)



and OMI/MLS for the year 2006, shows similar global morphology and seasonal variations in certain regions but with differences in some regions. In summary, the retrieval of tropospheric O<sub>3</sub> using SCIAMACHY limb-nadir matching observations has proved to be a reliable and powerful tool for studying tropospheric O<sub>3</sub> distributions, sources and sinks based on the comparisons conducted.

**Acknowledgements.** We thank the OMI/MLS, and TES teams for providing tropospheric O<sub>3</sub> data and making it available for comparison. We also thank the groups that provided the ozonesonde data, and acknowledge the WOUDC for archiving and making it available for use. We thank ESA and German Aerospace DLR for providing level 1 data for this study. This work was funded in parts by the German Aerospace DLR project SADOS (FKZ 50EE1105), by ESA through the SCIAMACHY Quality Working Group and by the University and State of Bremen, Germany. SCIAMACHY is jointly funded by Germany, the Netherlands and Belgium.

## References

- Aumann, H. H., Chahine, M. T., Gautier, C., Goldberg, M. D., Kalnay, E., McMillin, L. M., Revercomb, H., Rosenkranz, P. W., Smith, W. L., Staelin, D. H., Strow, L. L., and Susskind, J.: AIRS/AMSU/HSB on the Aqua mission: Design, science objectives, data products and processing systems, *IEEE T. Geosci. Remote*, 41, 253–264, 2003. 7816
- Beer, R.: TES on the Aura mission: Scientific objectives, measurements, and analysis overview, *IEEE T. Geosci. Remote*, 44, 1102–1105, 2006. 7819
- Beirle, S., Kühl, S., Pukite, J., and Wagner, T.: Retrieval of tropospheric column densities of NO<sub>2</sub> from combined SCIAMACHY nadir/limb measurements, *Atmos. Meas. Tech.*, 3, 283–299, doi:10.5194/amt-3-283-2010, 2010. 7816, 7824
- Bovensmann, H., Burrows, J. P., Buchwitz, M., Frerick, J., Noël, S., Rozanov, V. V., Chance, K. V., and Goede, A. H. P.: SCIAMACHY-Mission objectives and measurement modes, *J. Atmos. Sci.*, 56, 127–150, 1999. 7813, 7817, 7819
- Bovensmann, H., Eichmann, K. U., Noël, S., Flaud, J. M., Orphal, J., Monks P. S., Corlett G. K., Goede A. P. H., von Clarmann, T., Steck, T., Rozanov, V. V., and Burrows, J. P.: The Geostationary scanning imaging absorption spectrometer (GeoSCIA) as part of the Geostationary pollution explorer (GeoTROPE) mission: requirements concepts and capabilities, *Confer-*

## Tropospheric ozone retrievals from SCIAMACHY observations

F. Ebojje et al.

[Title Page](#)

[Abstract](#)

[Introduction](#)

[Conclusions](#)

[References](#)

[Tables](#)

[Figures](#)

◀

▶

[Back](#)

[Close](#)

[Full Screen / Esc](#)

[Printer-friendly Version](#)

[Interactive Discussion](#)



Coldewey-Egbers, M., Weber, M., Lamsal, L. N., de Beek, R., Buchwitz, M., and Burrows, J. P.: Total ozone retrieval from GOME UV spectral data using the weighting function DOAS approach, *Atmos. Chem. Phys.*, 5, 1015–1025, doi:10.5194/acp-5-1015-2005, 2005. 7823, 7826, 7828

5 Creilson, J. K., Fishman, J., and Wozniak, A. E.: Intercontinental transport of tropospheric ozone: a study of its seasonal variability across the North Atlantic utilizing tropospheric ozone residuals and its relationship to the North Atlantic Oscillation, *Atmos. Chem. Phys.*, 3, 2053–2066, doi:10.5194/acp-3-2053-2003, 2003. 7832

10 Creilson, J. K., Fishman, J., and Wozniak, A. E.: Arctic Oscillation-induced variability in satellite-derived tropospheric ozone, *Geophys. Res. Lett.*, 32, L14822, doi:10.1029/2005GL023016, 2005. 7832

15 Cuesta, J., Eremenko, M., Liu, X., Dufour, G., Hoepfner, M., Cai, Z., von Clarmann, T., Orphal, J., Chance, K., Spurr, R., and Flaud, J.-M.: Multi-spectral retrieval of lowermost tropospheric ozone combining IASI and GOME-2 satellite observations, in: Proceedings of ESA Advances in Atmospheric Science and Applications Conference, Bruges, Belgium, 2012. 7816

20 Eichmann, K.-U., von Savigny, C., Reichl, P., Robert, C., Steinwagner, J., Bovensmann, H., and Burrows, J. P.: SCODA: SCIAMACHY ClOud Detection Algorithm from limb radiance measurements Algorithm Theoretical Baseline Document (ATBD), Institute of Environmental Physics, University of Bremen, 2009. 7826

Fishman, J. and Balok, A. E.: Calculation of daily tropospheric ozone residuals using TOMS and empirically improved SBUV measurements: Application to an ozone pollution episode over the eastern United States, *J. Geophys. Res.*, 104, 30319–30340, 1999. 7815

25 Fishman, J. and Larsen, J. C.: Distribution of total ozone and stratospheric ozone in the tropics: Implications for the distribution of tropospheric ozone, *J. Geophys. Res.*, 92, 6627–6634, doi:10.1029/JD092iD06p06627, 1987. 7815

Fishman, J., Watson, C., Larsen, J., and Logan, J.: Distribution of tropospheric ozone determined from satellite data, *J. Geophys. Res.*, 95, 3599–3617, 1990. 7815

30 Fishman, J., Wozniak, A. E., and Creilson, J. K.: Global distribution of tropospheric ozone from satellite measurements using the empirically corrected tropospheric ozone residual technique: Identification of the regional aspects of air pollution, *Atmos. Chem. Phys.*, 3, 893–907, doi:10.5194/acp-3-893-2003, 2003. 7834, 7835

AMTD

6, 7811–7865, 2013

Tropospheric ozone retrievals from SCIAMACHY observations

F. Ebojje et al.

Title Page

Abstract

Introduction

Conclusions

References

Tables

Figures

◀

▶

Back

Close

Full Screen / Esc

Printer-friendly Version

Interactive Discussion



- Fishman, J., Creilson, J. K., Wozniak, A. E., and Crutzen, P. J.: Interannual variability of stratospheric and tropospheric ozone determined from satellite measurements, *J. Geophys. Res.*, 110, D20306, doi:10.1029/2005JD005868, 2005. 7832
- Flittner, D. E., Bhartia, P. K., and Herman, B. M., O<sub>3</sub> profiles retrieved from limb scatter measurements: Theory, *Geophys. Res. Lett.*, 27, 2601–2604, 2000. 7822
- Froidevaux, L., Jiang, Y. B., Lambert, A., Livesey, N. J., Read, W. G., Waters, J. W., Browell, E. V., Hair, J. W., Avery, M. A., McGee, T. J., Twigg, L. W., Sumnicht, G. K., Jucks, K. W., Margitan, J. J., Sen, B., Stachnik, R. A., Toon, G. C., Bernath, P. F., Boone, C. D., Walker, K. A., Filipiak, M. J., Harwood, R. S., Fuller, R. A., Manney, G. L., Schwartz, M. J., Daffer, W. H., Drouin, B. J., Cofield, R. E., Cuddy, D. T., Jarnot, R. F., Knosp, B. W., Perun, V. S., Snyder, W. V., Stek, P. C., Thurstans, R. P., and Wagner, P. A.: Validation of Aura Microwave Limb Sounder stratospheric ozone measurements, *J. Geophys. Res.*, 113, D15S20, doi:10.1029/2007JD008771, 2008. 7820
- Fussen, D. and Bingen, C.: A volcanism dependent model for the extinction profile of stratospheric aerosols in the UV-visible range, *Geophys. Res. Lett.*, 26, 703–706, 1999. 7822
- Gottwald, M. and Bovensmann, H. (Eds.): SCIAMACHY – Exploring the Changing Earth's Atmosphere, Springer Heidelberg Dordrecht London New York, ISBN:978-90-481-9895-5, doi:10.1007/978-90-481-9896-2, 2011. 7813, 7818
- Hilboll, A., Richter, A., Rozanov, A., Hodnebrog, Ø., Heckel, A., Solberg, S., Stordal, F., and Burrows, J. P.: Improvements to the retrieval of tropospheric NO<sub>2</sub> from satellite – stratospheric correction using SCIAMACHY limb/nadir matching and comparison to Oslo CTM2 simulations, *Atmos. Meas. Tech.*, 6, 565–584, doi:10.5194/amt-6-565-2013, 2013. 7816
- Hoinka, K. P.: Statistics of the global tropopause pressure, *Mon. Weather Rev.*, 126, 3303–3325, 1998. 7824
- Hoogen, R., Rozanov, V. V., Bramstedt, K., Eichmann, K. U., Weber, M., deBeek, R., Buchwitz, M., and Burrows, J. P.: Height resolved ozone information from GOME data, *Earth Observation Quarterly*, 58, 9–10, 1998. 7814, 7815
- Hoogen, R., Rozanov, V. V., and Burrows, J. P.: Ozone profiles from GOME satellite data: algorithm description and first validation, *J. Geophys. Res.*, 104, 8263–8280, 1999. 7814, 7815
- Kim, J. H. and Newchurch, M. J.: Climatology and trends of tropospheric ozone over the eastern Pacific Ocean: The influences of biomass burning and tropospheric dynamics, *Geophys. Res. Lett.*, 23, 3723–3726, doi:10.1029/96GL03615, 1996. 7832

Tropospheric ozone retrievals from SCIAMACHY observations

F. Ebojje et al.

Title Page

Abstract

Introduction

Conclusions

References

Tables

Figures



Back

Close

Full Screen / Esc

Printer-friendly Version

Interactive Discussion



Kim, J. H. and Newchurch, M. J.: Biomass-burning influence on tropospheric ozone over New Guinea and South America, *J. Geophys. Res.*, 103, 1455–1461, doi:10.1029/97JD02294, 1998. 7833

5 Kim, J. H., Newchurch, M. J., and Kunhee, H.: Distribution of Tropical Tropospheric Ozone Determined by the Scan-Angle Method Applied to TOMS Measurements, *J. Atmos. Sci.*, 58, 2699–2708, 2001. 7815

Kobayashi, J. and Toyama, Y.: On various methods of measuring the vertical distribution of atmospheric ozone (III) – Carbon iodine type chemical ozonesonde, *Pap. Met. Geophys.*, 17, 113–126, 1966. 7821

10 Koelemeijer, R. and Stammes, P.: Effects of clouds on ozone column retrieval from GOME UV measurements, *J. Geophys. Res.*, 104, 8281–8294, 1999. 7826

Kokhanovsky, A. A. and Rozanov, V. V.: The physical parameterization of the top-of-atmosphere reflection function for a cloudy atmosphere underlying surface system: the oxygen A-band case study, *J. Quant. Spectrosc. Ra.*, 85, 35–55, 2004. 7826

15 Komhyr, W. D.: Nonreactive gas sampling pump, *Rev. Sci. Instrum.*, 38, 981–983, 1967. 7820

Komhyr, W. D.: Electrochemical concentration cells for gas analysis, *Ann. Geoph.*, 25, 203–210,

1969. 7821

Komhyr, W. D.: Development of an ECC-Ozonesonde, *NOAA Techn. Rep. ERL 200-APCL 18ARL-149*, 1971. 7821

20 Kramarova, N. A., Frith, S. M., Bhartia, P. K., McPeters, R. D., Taylor, S. L., Fisher, B. L., Labow, G. J., and DeLand, M. T.: Validation of ozone monthly zonal mean profiles obtained from the version 8.6 Solar Backscatter Ultraviolet algorithm, *Atmos. Chem. Phys.*, 13, 6887–6905, doi:10.5194/acp-13-6887-2013, 2013. 7815

25 Ladstätter-Weißenmayer, A., Meyer-Arnek, J., Schlemm, A., and Burrows, J. P.: Influence of stratospheric airmasses on tropospheric vertical O<sub>3</sub> columns based on GOME (Global Ozone Monitoring Experiment) measurements and backtrajectory calculation over the Pacific, *Atmos. Chem. Phys.*, 4, 903–909, doi:10.5194/acp-4-903-2004, 2004. 7815

Lawrence, M. G. and Crutzen, P. J.: Influence of NO<sub>x</sub> emissions from ships on tropospheric photochemistry and climate, *Nature*, 402, 167–170, 1999. 7833

30 Levelt, P. F., van den Oord, G. H. J., Dobber, M. R., Ilkki, A., Visser, H., de Vries, J., Stammes, P., Lundell, J. O. V., and Saari, H.: The Ozone Monitoring Instrument, *IEEE T. Geosci. Remote*, 44, 1093–1101, 2006. 7819

Tropospheric ozone retrievals from SCIAMACHY observations

F. Ebojje et al.

[Title Page](#)

[Abstract](#)

[Introduction](#)

[Conclusions](#)

[References](#)

[Tables](#)

[Figures](#)

◀

▶

[Back](#)

[Close](#)

[Full Screen / Esc](#)

[Printer-friendly Version](#)

[Interactive Discussion](#)



- Liu, C., Penning de Vries, M., Beirle, S., Hoor, P., Marbach, T., Frankenberg, C., Platt, U., and Wagner T.: Relationship between ATSR fire counts and CO vertical column densities retrieved from SCIAMACHY onboard ENVISAT, *Remote Sens. of Fire: Sc. and App.*, Proc. of SPIE Vol. 7089, 70890I, doi:10.1117/12.793283, 2008. 7833
- Liu, X., Chance, K., Sioris, C. E., Spurr, R. J. D., Kurosu, T. P., Martin, R. V., and Newchurch, M. J.: Ozone profile and tropospheric ozone retrievals from the Global Ozone Monitoring Experiment: Algorithm description and validation, *J. Geophys. Res.*, 110, D20307, doi:10.1029/2005JD006240, 2005. 7833
- Liu, X., Chance, K., Sioris, C. E., Kurosu, T. P., Spurr, R. J. D., Martin, R. V., Fu, T. M., Logan, J. A., Jacob, D. J., Palmer, P. I., Newchurch, M. J., Megretskaya, I. A., and Chatfield, R., First directly retrieved global distribution of tropospheric column ozone from GOME: Comparison with the GEOS-CHEM model, *J. Geophys. Res.*, 111, D02308, doi:10.1029/2005JD006564, 2006. 7815
- Liu, X., Bhartia, P. K., Chance, K., Spurr, R. J. D., and Kurosu, T. P.: Ozone profile retrievals from the Ozone Monitoring Instrument, *Atmos. Chem. Phys.*, 10, 2521–2537, doi:10.5194/acp-10-2521-2010, 2010. 7815
- Logan, J. A. and Kirchhoff, V. W. J. H.: Seasonal variations of tropospheric ozone at Natal, Brazil, *J. Geophys Res.*, 91, 7875–7881, 1986. 7833
- Lucke, R. L., Korwan, D. R., Bevilacqua, R. M., Hornstein, J. S., Shettle, E. P., Chen, D. T., Daehler, M., Lumpe, J. D., Fromm, M. D., Debristian, D., Neff, B., Squire, M., König-Langlo, G., and Davies J.: The polar ozone and aerosol measurement (POAM) III instrument and early validation results, *J. Geophys. Res.*, 104, 18785–18799, 1999. 7814
- Mariotti, A., Moustaqi, M., Legras, B., and Teitelbaum, H.: Comparison between vertical ozone soundings and reconstructed potential vorticity maps by contour advection with surgery, *J. Geophys. Res.*, 102, 6131–6142, doi:10.1029/96JD03509, 1997. 7830
- Matthews, E.: Vegetation, Land-Use and Seasonal Albedo Data Sets, in: *Global Change Data Base Africa Documentation*, Appendix D, NOAA/NGDC, 1984. 7822
- McCormick, M. P., Zawodny, J. M., Veiga, R. E., Larsen, J. C., and Wang P.-H.: An overview of SAGE I and II ozone measurements, *Planet. Space Sci.*, 37, 1567–1586, 1989. 7814
- McPeters, R. D., Janz, S. J., Hilsenrath, H., and Brown, T. L.: The retrieval of  $O_3$  profiles from limb scatter measurements: Results from the shuttle ozone limb sounding experiment, *Geophys. Res. Lett.*, 27, 2597–2600, 2000. 7814

## Tropospheric ozone retrievals from SCIAMACHY observations

F. Ebojje et al.

[Title Page](#)

[Abstract](#)

[Introduction](#)

[Conclusions](#)

[References](#)

[Tables](#)

[Figures](#)

◀

▶

[Back](#)

[Close](#)

[Full Screen / Esc](#)

[Printer-friendly Version](#)

[Interactive Discussion](#)



Meijer, Y., Swart, D. P. J., Baier, F., Barthia, P. K., Bodeker, G. E., Casadio, S., Chance, K., del Frate, F., Ebetseder, T., Flynn, L. E., Godin-Beekmann, S., Hansen, G., Hasekamp, O. P., Kaifel, A., Kelder, H. M., Kerridge, B. J., Lambert, J.-C., Landgraf, J., Latter, B., Liu, X., McDermid, I. S., Müller, M. D., Pachepsky, Y., Rozanov, V., Siddans, R., Tellmann, S., van der A, R. J., van Oss, R. F., Weber, M., and Zehner, C.: Evaluation of GOME ozone profiles from nine different algorithms, *J. Geophys. Res.*, 111, D21306, doi:10.1029/2005JD006778, 2006. 7814

Mieruch, S., Weber, M., von Savigny, C., Rozanov, A., Bovensmann, H., Burrows, J. P., Bernath, P. F., Boone, C. D., Froidevaux, L., Gordley, L. L., Mlynczak, M. G., Russell III, J. M., Thomason, L. W., Walker, K. A., and Zawodny, J. M.: Global and long-term comparison of SCIAMACHY limb ozone profiles with correlative satellite data (2002–2008), *Atmos. Meas. Tech.*, 5, 771–788, doi:10.5194/amt-5-771-2012, 2012.

Mount, G. H., Rusch, D. W., Noxon, J. F., Zawodny, J. M., and Barth, C. A.: Measurements of stratospheric NO<sub>2</sub> from the Solar Mesosphere Explorer satellite: 1. An overview of the results, *J. Geophys. Res.*, 2, 89, 1327–1340, 1984. 7814

Munro, R., Siddans, R., Reburn, W. J., and Kerridge, B.: Direct measurement of tropospheric ozone from space, *Nature*, 392, 168–171, 1998. 7815

Munro, R., Eisinger, M., Anderson, C., Callies, J., Corpaccioli, E., Lang, R., Lefebvre, A., Livschitz, Y., and Perez Albinana, A.: GOME-2 on MetOp: From in-orbit verification to routine operations, in: Proceedings of EUMETSAT Meteorological Satellite Conference, Helsinki, Finland, 12–16 June, 2006. 7813

Newchurch, M. J., Liu, X., Kim, J. H., and Bhartia, P. K.: On the accuracy of total ozone mapping spectrometer retrievals over tropical cloudy regions, *J. Geophys. Res.*, 106, 32315–32326, 2001. 7826

Rahpoe, N., von Savigny, C., Weber, M., Rozanov, A.V., Bovensmann, H., and Burrows, J. P.: Error budget analysis of SCIAMACHY limb ozone profile retrievals using the SCIATRAN model, *Atmos. Meas. Tech. Discuss.*, 6, 4645–4676, doi:10.5194/amtd-6-4645-2013, 2013. 7827

Ran, L., Zhao, C. S., Xu, W. Y., Han, M., Lu, X. Q., Han, S. Q., Lin, W. L., Xu, X. B., Gao, W., Yu, Q., Geng, F. H., Ma, N., Deng, Z. Z., and Chen, J.: Ozone production in summer in the megacities of Tianjin and Shanghai, China: a comparative study, *Atmos. Chem. Phys.*, 12, 7531–7542, doi:10.5194/acp-12-7531-2012, 2012. 7833

## Tropospheric ozone retrievals from SCIAMACHY observations

F. Ebojje et al.

[Title Page](#)

[Abstract](#)

[Introduction](#)

[Conclusions](#)

[References](#)

[Tables](#)

[Figures](#)

◀

▶

[Back](#)

[Close](#)

[Full Screen / Esc](#)

[Printer-friendly Version](#)

[Interactive Discussion](#)



Rodgers, C. D.: Inverse Methods for Atmospheric Sounding: Theory and Practice, Atm., Oceanic and Plan. Phy., World Sci., Singapore, 2000. 7815, 7819

Rohen, G. J.: Retrieval of Upper Stratospheric and Lower Mesospheric Ozone Profiles from SCIAMACHY Limb Scatter Measurements and Observations of the Ozone Depletion During the Solar Proton Event in October and November 2003, Logos Publication, Berlin, PhD. thesis, ISBN:978-3-3825-1363-4, ISSN:1615-6862, 2006. 7822

Rozanov, A., Rozanov, V., Buchwitz, M., Kokhanovsky, A., and Burrows, J. P.: SCIATRAN 2.0 – a new radiative transfer model for geophysical applications, *Adv. Space Res.*, 36, 1015–1019, 2005. 7822

Rozanov, V. V., Kurosu, T., and Burrows, J. P.: Retrieval of Atmospheric Constituents in the UV Visible: A New Quasi-Analytical Approach for the Calculation of Weighting Functions, *J. Quant. Spectrosc. Ra.*, 60, 277–299, 1998. 7823

Rusch, D. W., Mount, G. H., Barth, C. A., Thomas, R. J., and Callan, M. T.: Solar mesospheric explorer ultraviolet spectrometer: Measurements of ozone in the 1.0–0.1 mbar region, *J. Geophys. Res.*, 89, 677–687, 1984. 7814

Russell III, J. M., Gordley, L. L., Park, J. H., Drayson, S. R., Hesketh, W. D., Cicerone, R. J., Tuck, A. F., Frederick, J. E., Harries, J. E., and Crutzen, P. J.: The halogen occultation experiment, *J. Geophys. Res.*, 98, 10777–10797, 1993. 7814

Schoeberl, M. R., Ziemke, J. R., Bojkov, B., Livesey, N., Duncan, B., Strahan, S., Froidevaux, L., Kulawik, S., Bhartia, P. K., Chandra, S., Levelt, P. F., Witte, J. C., Thompson, A. M., Cuevas, E., Redondas, A., Tarasick, D. W., Davies, J., Bodeker, G., Hansen, G., Johnson, B. J., Oltmans, S. J., Vomel, H., Allaart, M., Kelder, H., Newchurch, M., Godin-Beekmann, S., Ancellet, G., Claude, H., Andersen, S. B., Kyro, E., Parrondos, M., Yela, M., Zablocki, G., Moore, D., Dier, H., von der Gathen, P., Viatte, P., Stubi, R., Calpini, B., Skrivankova, P., Dorokhov, V., De Backer, H., Schmidlin, F. J., Coetzee, G., Fujiwara, M., Thouret, V., Posny, F., Morris, G., Merrill, J., Leong, C. P., Koenig-Langlo, G., and Joseph, E.: A trajectory-based estimate of the tropospheric ozone column using the residual method, *J. Geophys. Res.*, 112, D24S49, doi:10.1029/2007JD008773, 2007. 7815

Sierk, B., Richter, A., Rozanov, A., v. Savigny, C., Schmoltner, A. M., Buchwitz, M., Bovensmann, H., and Burrows, J. P.: Retrieval and Monitoring of Atmospheric Trace Gas Concentrations in Nadir and Limb Geometry using the Space-Borne SCIAMACHY Instrument, *Environ. Monitor. Assess.*, 120, 65–77, doi:10.1007/s10661-005-9049-9, 2006. 7816, 7824

AMTD

6, 7811–7865, 2013

## Tropospheric ozone retrievals from SCIAMACHY observations

F. Ebojje et al.

Title Page

Abstract

Introduction

Conclusions

References

Tables

Figures

◀

▶

◀

▶

Back

Close

Full Screen / Esc

Printer-friendly Version

Interactive Discussion



## Tropospheric ozone retrievals from SCIAMACHY observations

F. Ebojje et al.

[Title Page](#)

[Abstract](#)

[Introduction](#)

[Conclusions](#)

[References](#)

[Tables](#)

[Figures](#)

◀

▶

◀

▶

[Back](#)

[Close](#)

[Full Screen / Esc](#)

[Printer-friendly Version](#)

[Interactive Discussion](#)

Singer, S. F. and Wentworth, R. C.: A method for the determination of the vertical ozone distribution from a satellite, *J. Geophys. Res.*, 62, 299–308, doi:10.1029/JZ062i002p00299, 1957. 7815

Sioris, C. E., Kurosu, T. P., Martin, R. V., and Chance, K.: Stratospheric and tropospheric NO<sub>2</sub> observed by SCIAMACHY: First results, *Adv. Space Res.*, 34, 780–785, 2004. 7816

Smit, H. G. J.: Ozonesondes, in *Encyclopedia of Atmospheric Sciences*, edited by: Holton, J., Pyle, J., and Curry, J., 1469–1476, Academic Press, London, 2002. 7821

Smit, H. G. J., Straeter, W., Johnson, B. J., Oltmans, S. J., Davies, J., Tarasick, D. W., Hoegger, B., Stubi, R., Schmidlin, F. J., Northam, T., Thompson, A. M., Witte, J. C., Boyd, I., and Posny, F.: Assessment of the performance of ECCozonesondes under quasiflight conditions in the environmental simulation chamber: Insights from the Juelich Ozone Sonde Intercomparison Experiment (JOSIE), *J. Geophys. Res.*, 112, D19306, doi:10.1029/2006JD007308, 2007. 7821

Sonkaew, T., Rozanov, V. V., von Savigny, C., Rozanov, A., Bovensmann, H., and Burrows, J. P.: Cloud sensitivity studies for stratospheric and lower mesospheric ozone profile retrievals from measurements of limb scattered solar radiation, *Atmos. Meas. Tech. Discuss.*, 2, 379–438, doi:10.5194/amtd-2-379-2009, 2009. 7822

Thompson, A. M. and Hudson, R. D.: Tropical tropospheric ozone (TTO) maps from Nimbus 7 and Earth Probe TOMS by the modified-residual method: Evaluation with sondes, ENSO signals, and trends from Atlantic regional time series, *J. Geophys. Res.*, 104, 26961–26975, doi:10.1029/1999JD900470, 1999. 7815

Thompson, A. M., Witte, J. C., McPeters, R. D., Oltmans, S. J., Schmidlin, F. J., Logan, J. A., Fujiwara, M., Kirchhoff, V. W. J. H., Posny, F., Coetzee, G. J. R., Hoegger, B., Kawakami, S., Ogawa, T., Johnson, B. J., Vomel, H., and Labow, G. J.: Southern Hemisphere Additional Ozonesondes (SHADOZ) 1998–2000 tropical ozone climatology: 1. Comparison with Total Ozone Mapping Spectrometer (TOMS) and ground-based measurements, *J. Geophys. Res.*, 108, 8238, doi:10.1029/2001JD000967, 2003. 7821

Valks, P., Koelemeijer, R. B. A., van Weele, M., van Velthoven, P., Fortuin, J. P. F., and Kelder, H.: Variability in tropical tropospheric ozone: Analysis with Global Ozone Monitoring Experiment observations and a global model, *J. Geophys. Res.*, 108, 4328, doi:10.1029/2002JD002894, 2003. 7832

von Savigny, C., Haley, C. S., Sioris, C. E., McDade, I. C., Llewellyn, E. J., Degenstein, D., Evans, W. F. J., Gattinger, R. L., Griffioen, E., Kyrölä, E., Lloyd, N. D., McConnell, J. C.,

- McLinden, C. A., Mégie, G., Murtagh, D. P., Solheim, B., and Strong, K.: Stratospheric ozone profiles retrieved from limb scattered sunlight radiance spectra measured by the OSIRIS instrument on the Odin satellite, *Geophys. Res. Lett.*, 30, 1755, doi:10.1029/2002GL016401, 2003. 7822
- 5 Wagner, T., Beirle, S., Deutschmann, T., Eigemeier, E., Frankenberg, C., Grzegorski, M., Liu, C., Marbach, T., Platt, U., and Penning de Vries, M.: Monitoring of atmospheric trace gases, clouds, aerosols and surface properties from UV/vis/NIR satellite instruments, *J. Opt. A., Pure Appl. Opt.*, 10, 104019, doi:10.1088/1464-4258/10/10/104019, 2008. 7813
- Weber, M., Lamsal, L. N., Coldewey-Egbers, M., Bramstedt, K., and Burrows, J. P.: Pole-to-pole validation of GOME WFDOAS total ozone with groundbased data, *Atmos. Chem. Phys.*, 5, 10 1341–1355, doi:10.5194/acp-5-1341-2005, 2005. 7823, 7826, 7828
- Weber, M., Lamsal, L. N., and Burrows, J. P.: Improved SCIAMACHY WFDOAS total ozone retrieval: Steps towards homogenising long-term total ozone datasets from GOME, SCIAMACHY, and GOME2, Proc. "Envisat Symposium 2007", Montreux, Switzerland, 23–27 April 15 2007, ESA SP-636, 2007. 7823
- WMO: Meteorology – A three dimensional science. *WMO Bull.*, 6, 134–138, 1957. 7824
- World Meteorological Organization, Scientific Assessment of Ozone Depletion: 1998, Global Ozone Research and Monitoring Project – Report No. 44, Geneva, 1999. 7821
- Ziemke, J. R., Chandra, S., and Bhartia, P. K.: Two new methods for deriving tropospheric column ozone from TOMS measurements: Assimilated UARS MLS/HALOE and convective-cloud differential techniques, *J. Geophys. Res.*, 103, 22115–22128, 1998. 7815
- Ziemke, J. R., Chandra, S., Duncan, B. N., Froidevaux, L., Bhartia, P. K., Levelt, P. F., and Waters, J. W.: Tropospheric ozone determined from Aura OMI and MLS: Evaluation of measurements and comparison with the Global Modeling Initiative's Chemical Transport Model, *J. Geophys. Res.*, 111, D19303, doi:10.1029/2006JD007089, 2006. 7815
- Ziemke, J. R., Chandra, S., Labow, G. J., Bhartia, P. K., Froidevaux, L., and Witte, J. C.: A global climatology of tropospheric and stratospheric ozone derived from Aura OMI and MLS measurements, *Atmos. Chem. Phys.*, 11, 9237–9251, doi:10.5194/acp-11-9237-2011, 2011. 25 7815, 7820

## Tropospheric ozone retrievals from SCIAMACHY observations

F. Ebojje et al.

[Title Page](#)[Abstract](#)[Introduction](#)[Conclusions](#)[References](#)[Tables](#)[Figures](#)[◀](#)[▶](#)[Back](#)[Close](#)[Full Screen / Esc](#)[Printer-friendly Version](#)[Interactive Discussion](#)

## Tropospheric ozone retrievals from SCIAMACHY observations

F. Ebojie et al.

**Table 1.** Monthly average and errors in tropospheric ozone columns, stratospheric ozone columns, total ozone columns and the effect of the tropopause height in 2003.

Month	Mean Tropospheric Column Ozone	Resulting error in Tropospheric Column Ozone DU	Mean Stratospheric Column Ozone DU	Error of Stratospheric Column Ozone %	Mean Total Column Ozone	Error of Total Column Ozone DU	Mean Tropopause Height	Ozone error caused by Tropopause Height error DU %				
Jan	26.87	5.5	20.4	258.44	4.6	1.8	285.78	2.9	1.0	12.34	0.1	0.8
Feb	26.30	5.6	21.4	265.23	4.7	1.8	293.26	2.9	1.0	12.30	0.1	0.9
Mar	27.07	5.8	21.5	275.49	4.9	1.8	303.82	3.0	1.0	12.12	0.1	0.6
Apr	28.57	6.0	21.0	282.82	5.1	1.8	312.83	3.1	1.0	12.04	0.1	0.8
May	31.38	5.8	18.5	275.86	4.8	1.8	309.38	3.1	1.0	12.00	0.1	0.5
Jun	32.58	5.7	17.3	263.68	4.7	1.8	298.20	3.0	1.0	12.35	0.1	0.4
Jul	31.69	5.7	17.9	261.83	4.8	1.8	295.12	3.0	1.0	12.29	0.1	0.4
Aug	34.50	5.8	16.8	260.57	4.9	1.9	296.09	3.0	1.0	12.30	0.1	0.3
Sep	33.76	5.6	16.5	255.29	4.7	1.8	291.04	2.9	1.0	12.29	0.1	0.3
Oct	33.15	5.5	16.7	256.15	4.6	1.8	293.95	2.9	1.0	12.10	0.1	0.4
Nov	31.98	5.3	16.6	252.29	4.4	1.7	286.95	2.9	1.0	12.13	0.1	0.4
Dec	32.90	5.4	16.5	253.86	4.5	1.8	288.76	2.9	1.0	12.19	0.1	0.6

**Tropospheric ozone retrievals from SCIAMACHY observations**

F. Ebojje et al.

**Table 2.** RMS error in [%] from stratospheric ozone profile retrieval parameters at northern mid-latitudes: [35°–45° N].

Parameter	Bias	10 km	15 km	20 km	25 km	30 km	35 km	40 km
Albedo	0.1	3.21	1.42	0.87	0.58	0.45	0.30	0.03
Aerosol	40 %	4.38	4.91	0.84	2.42	0.38	0.41	0.02
Pressure	2 %	1.97	1.37	1.66	1.82	1.87	1.91	2.05
Temperature	2 K	0.87	0.75	0.88	0.86	0.74	0.75	0.71
Tangent Height	200 m	4.00	3.40	0.76	1.53	1.63	2.12	3.39
Cross Section	2 % (p,T)	0.11	0.25	0.24	0.02	0.16	0.17	0.29

- [Title Page](#)
- [Abstract](#) [Introduction](#)
- [Conclusions](#) [References](#)
- [Tables](#) [Figures](#)
- [◀](#) [▶](#)
- [◀](#) [▶](#)
- [Back](#) [Close](#)
- [Full Screen / Esc](#)

[Printer-friendly Version](#)[Interactive Discussion](#)

**Tropospheric ozone retrievals from SCIAMACHY observations**

F. Ebojje et al.

**Table 3.** RMS error in [%] from stratospheric ozone profile retrieval parameters at northern high latitudes: [65° - 75° N].

Parameter	Bias	10 km	15 km	20 km	25 km	30 km	35 km	40 km
Albedo	0.1	2.02	0.81	0.38	0.23	0.21	0.11	0.02
Aerosol	40 %	15.56	2.64	3.69	1.07	0.19	0.33	0.12
Pressure	2 %	2.57	1.59	1.89	2.13	2.17	2.22	2.41
Temperature	2 K	1.14	0.88	1.01	1.01	0.87	0.87	0.81
Tangent Height	200 m	4.52	3.83	0.10	3.15	2.31	2.69	3.95
Cross Section	2 % (p,T)	0.11	0.30	0.28	0.02	0.18	0.19	0.35

<a href="#">Title Page</a>	
<a href="#">Abstract</a>	<a href="#">Introduction</a>
<a href="#">Conclusions</a>	<a href="#">References</a>
<a href="#">Tables</a>	<a href="#">Figures</a>
<a href="#">◀</a>	<a href="#">▶</a>
<a href="#">◀</a>	<a href="#">▶</a>
<a href="#">Back</a>	<a href="#">Close</a>
<a href="#">Full Screen / Esc</a>	

[Printer-friendly Version](#)[Interactive Discussion](#)

**Table 4.** Comparisons of tropospheric ozone columns from SCIAMACHY, ozonesondes, TES and OMI/MLS for some selected sondes stations over the entire time series (2004–2011).

Station name	Collocated points	Mean value of trop. O <sub>3</sub> from SCIAMACHY (DU)			Mean value of trop. O <sub>3</sub> from sondes (DU)	Mean value of trop. O <sub>3</sub> from TES (DU)	Mean value of trop. O <sub>3</sub> from OM/MLS (DU)	Mean value of trop. O <sub>3</sub> rel. diff. (SCIAMACHY)	Mean value of trop. O <sub>3</sub> rel. diff. (TES)	Mean value of trop. O <sub>3</sub> rel. diff. (OM/MLS)
		Latitude	Longitude	Mean value of trop. O <sub>3</sub> (DU)						
1. Lerwick	62	60.13	358.82	40.61 ± 6.82	33.36 ± 4.70	38.21 ± 2.64	30.05 ± 4.11	0.22	0.15	-0.10
2. Churchill	57	58.75	265.93	34.79 ± 7.55	31.23 ± 4.55	35.44 ± 2.38	30.20 ± 4.53	0.11	0.13	-0.03
3. Edmonton	62	53.55	245.90	34.43 ± 5.45	28.29 ± 3.85	34.43 ± 2.37	25.94 ± 3.26	0.22	0.22	-0.08
4. Goose Bay	59	53.32	299.70	34.75 ± 6.75	32.06 ± 5.22	37.99 ± 2.82	30.72 ± 3.16	0.08	0.18	-0.04
5. Legionowo	71	52.40	20.97	38.18 ± 4.92	36.11 ± 6.97	41.14 ± 4.86	28.98 ± 4.48	0.06	0.14	-0.20
6. DeBilt	75	52.10	5.18	41.34 ± 6.90	35.37 ± 5.48	41.19 ± 4.15	29.69 ± 4.06	0.17	0.16	-0.16
7. Valentia	48	51.93	349.75	34.87 ± 3.62	37.35 ± 5.06	40.83 ± 3.12	31.45 ± 4.22	-0.07	0.09	-0.16
8. Uccle	78	50.80	4.35	41.35 ± 6.77	35.69 ± 6.17	41.29 ± 4.34	29.77 ± 4.02	0.16	0.16	-0.17
9. Bratts Lake	78	50.20	255.30	33.89 ± 4.25	32.69 ± 5.19	37.79 ± 4.09	26.94 ± 3.10	0.04	0.16	-0.18
10. Praha	26	50.02	14.45	38.75 ± 4.75	34.36 ± 4.75	38.30 ± 3.01	27.00 ± 3.84	0.13	0.11	-0.21
11. Kelowna	77	49.93	240.60	33.34 ± 5.07	32.94 ± 5.19	36.18 ± 2.82	26.15 ± 3.85	0.01	0.10	-0.21
12. Payerne	82	46.49	6.57	43.93 ± 6.40	33.61 ± 6.17	41.67 ± 5.21	29.53 ± 4.58	0.31	0.24	-0.12
13. Egbert	74	44.23	280.22	37.82 ± 4.88	37.37 ± 7.23	42.85 ± 5.42	30.81 ± 5.03	0.01	0.15	-0.18
14. Yarmouth	63	43.87	293.89	40.45 ± 6.44	38.94 ± 7.75	43.06 ± 5.46	32.45 ± 5.73	0.04	0.11	-0.17
15. Sapporo	82	43.10	141.30	40.39 ± 8.87	35.29 ± 8.70	42.58 ± 6.29	34.26 ± 6.51	0.14	0.21	-0.03
16. Madrid	81	40.45	356.28	40.29 ± 5.62	34.76 ± 6.37	41.22 ± 5.10	31.08 ± 6.34	0.16	0.21	-0.11
17. Ankara	78	39.95	32.88	39.35 ± 5.63	35.64 ± 9.92	44.59 ± 9.16	33.18 ± 8.50	0.10	0.25	-0.07
18. Wallops Island	79	37.93	284.52	42.36 ± 6.03	41.47 ± 8.09	45.46 ± 5.52	33.10 ± 6.70	0.04	0.10	-0.20
19. Tsukuba	82	36.10	140.10	41.69 ± 7.33	41.47 ± 9.30	45.08 ± 3.64	33.87 ± 6.22	0.01	0.09	-0.18
20. Huntsville	38	34.72	273.36	40.11 ± 5.29	40.29 ± 8.42	44.96 ± 4.86	32.39 ± 7.16	-0.00	0.12	-0.28
21. Isfahan	50	32.51	51.70	32.96 ± 4.65	37.31 ± 9.11	41.80 ± 4.94	31.03 ± 6.56	-0.12	0.12	-0.17
22. Naha	82	26.20	127.70	39.88 ± 6.58	38.91 ± 7.74	39.42 ± 4.80	32.56 ± 4.84	0.02	0.01	-0.16
23. Hong Kong	81	22.31	114.17	38.58 ± 6.31	38.89 ± 6.27	39.11 ± 3.95	32.59 ± 4.38	-0.01	0.01	-0.16
24. Hahol	47	21.01	105.80	34.81 ± 4.32	36.83 ± 5.87	38.08 ± 3.76	30.09 ± 4.24	-0.05	0.03	-0.18
25. Hilo	77	19.43	204.98	33.75 ± 4.74	33.59 ± 6.19	36.42 ± 4.68	29.09 ± 4.72	0.00	0.08	-0.13
26. Costarica	67	9.98	275.79	25.30 ± 4.38	25.26 ± 3.55	29.17 ± 1.69	25.08 ± 2.24	0.00	0.15	-0.01
27. Paramaribo	69	5.81	304.79	26.15 ± 5.12	26.25 ± 6.54	29.92 ± 2.56	25.11 ± 2.60	-0.00	0.14	-0.04
28. Sepang Airport	62	2.73	101.70	25.49 ± 5.25	24.80 ± 3.88	24.56 ± 2.28	20.90 ± 3.13	0.03	-0.01	-0.16
29. San Cristobal	31	-0.92	270.38	27.36 ± 4.97	25.80 ± 5.69	29.06 ± 3.72	22.25 ± 3.79	0.06	0.13	-0.02
30. Nairobi	69	-1.27	36.80	26.99 ± 3.40	28.16 ± 3.63	33.54 ± 3.33	27.32 ± 2.85	-0.04	0.19	-0.03
31. Natal	72	-5.49	324.74	29.06 ± 5.27	34.43 ± 8.30	36.79 ± 7.23	31.04 ± 5.73	-0.16	0.07	-0.10
32. Java	67	-7.50	112.60	23.92 ± 3.86	23.72 ± 6.54	25.12 ± 4.14	21.65 ± 4.06	0.01	0.06	-0.09
33. Watukosek	52	-7.57	112.65	24.49 ± 4.37	23.40 ± 6.45	25.06 ± 4.25	22.02 ± 4.26	0.07	0.07	-0.06
34. Ascension Island	63	-7.98	345.58	32.42 ± 8.56	38.22 ± 7.67	40.45 ± 6.39	34.64 ± 5.35	-0.15	0.06	-0.09
35. Samoa	71	-14.23	189.44	24.97 ± 4.89	22.21 ± 5.66	23.86 ± 4.15	19.60 ± 3.97	0.12	0.07	-0.12
36. Fiji	43	-18.13	178.40	29.97 ± 5.38	23.89 ± 7.43	27.76 ± 4.97	22.98 ± 4.20	0.25	0.16	-0.04
37. LaReunion Island	72	-21.06	55.48	35.38 ± 6.05	41.12 ± 8.56	39.98 ± 6.79	33.62 ± 5.96	-0.14	-0.03	-0.18
38. Irene	31	-25.90	28.22	33.75 ± 6.69	37.84 ± 7.05	38.46 ± 5.20	32.06 ± 4.67	-0.11	0.02	0.15
39. Broadmeadows	62	-37.68	144.95	31.22 ± 6.36	29.06 ± 4.98	31.18 ± 2.97	26.23 ± 3.19	0.07	0.07	-0.10
40. Lauder	50	-45.04	169.68	27.76 ± 5.80	23.06 ± 3.16	25.45 ± 2.23	22.48 ± 2.55	0.20	0.10	-0.03
41. Macquarie Island	62	-54.50	158.97	26.04 ± 4.78	22.68 ± 3.36	23.15 ± 3.52	25.36 ± 4.20	0.15	0.02	0.12
42. Ushuaia	21	-54.85	291.68	25.20 ± 5.90	21.01 ± 3.59	23.75 ± 3.19	25.15 ± 3.52	0.20	0.13	0.20
43. Marambio	45	-64.23	303.38	21.31 ± 4.34	19.04 ± 3.97	21.38 ± 6.19	22.93 ± 4.27	0.12	0.12	0.20
Mean value of tropospheric ozone				33.74 ± 5.7	32.18 ± 6.1	35.78 ± 4.3	28.52 ± 4.5	0.06	0.11	-0.10

# Tropospheric ozone retrievals from SCIAMACHY observations

F. Ebojje et al.

Title Page

## Abstract

## Introduction

## Conclusion

## References

Tables

## Figures



Back

**Close**

Full Screen / Esc

#### Interactive Discussion

## Tropospheric ozone retrievals from SCIAMACHY observations

F. Ebojie et al.

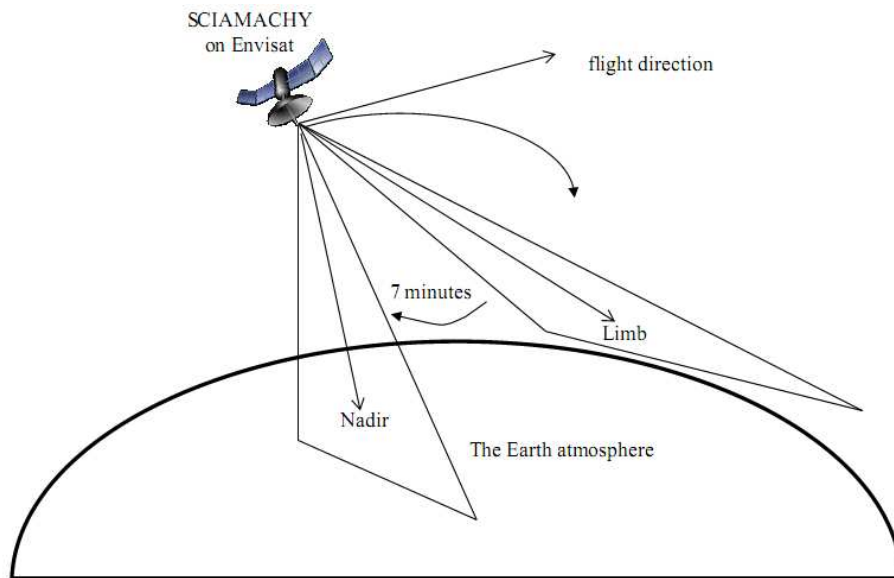


**Fig. 1.** Illustration of SCIAMACHY limb and nadir observation geometries.

[Title Page](#)

[Abstract](#)

[Introduction](#)

[Conclusions](#)

[References](#)

[Tables](#)

[Figures](#)

◀

▶

◀

▶

[Back](#)

[Close](#)

[Full Screen / Esc](#)

[Printer-friendly Version](#)

[Interactive Discussion](#)

## Tropospheric ozone retrievals from SCIAMACHY observations

F. Ebojje et al.

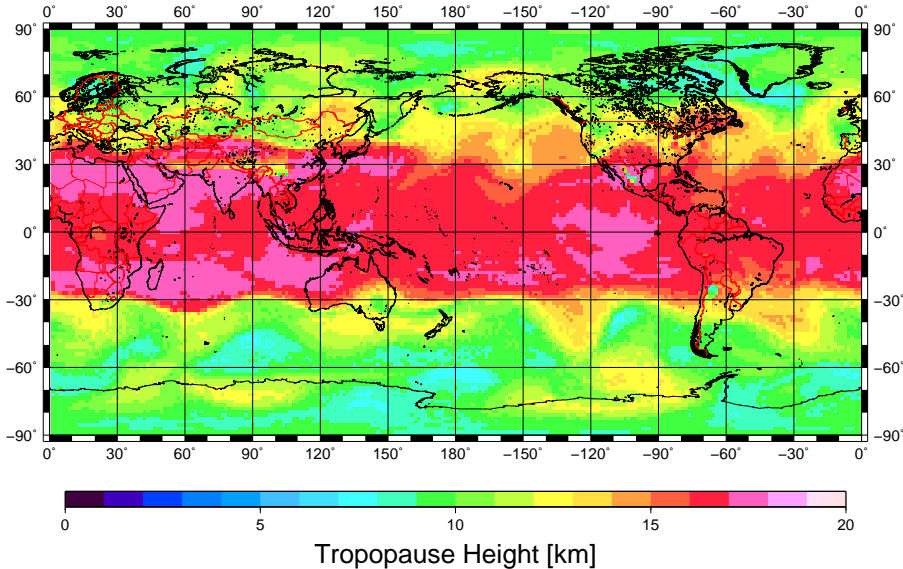


**Fig. 2.** Distribution of global tropopause height in 28 June 2005.

[Title Page](#)

[Abstract](#)

[Introduction](#)

[Conclusions](#)

[References](#)

[Tables](#)

[Figures](#)

◀

▶

◀

▶

[Back](#)

[Close](#)

[Full Screen / Esc](#)

[Printer-friendly Version](#)

[Interactive Discussion](#)

## Tropospheric ozone retrievals from SCIAMACHY observations

F. Ebojie et al.

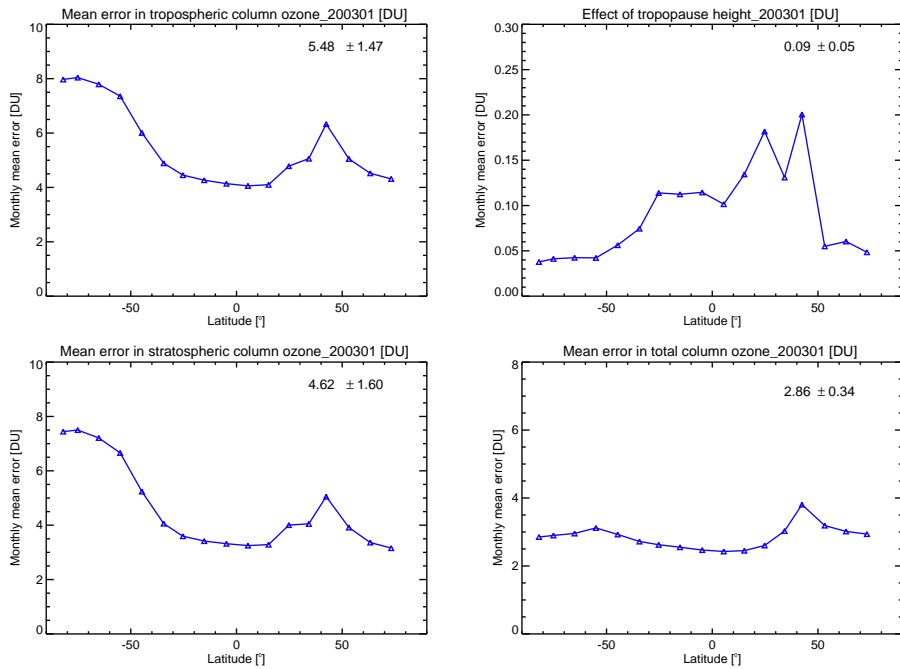


**Fig. 3.** Top panels from left to right: monthly and zonal mean error in tropospheric ozone columns, monthly and zonal mean error in tropospheric ozone columns associated with error in tropopause height. Bottom panels from left to right: monthly and zonal mean error of the stratospheric ozone columns, monthly and zonal mean error of total column ozone in January 2003.

## Tropospheric ozone retrievals from SCIAMACHY observations

F. Ebojie et al.

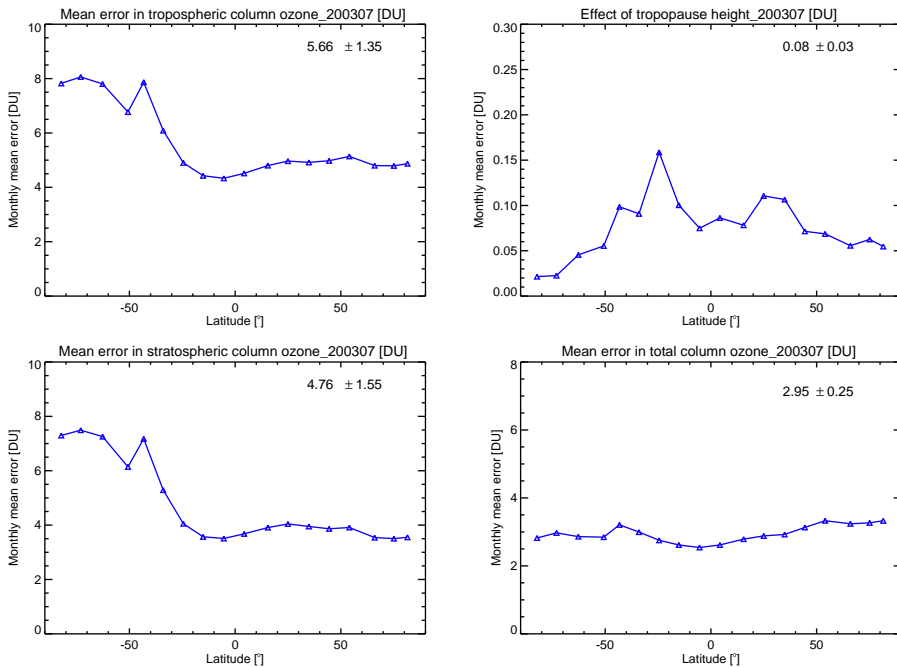


**Fig. 4.** Same as Fig. 3 but for July 2003.

Title Page

Abstract

Introduction

Conclusions

References

Tables

Figures

◀

▶

◀

▶

Back

Close

Full Screen / Esc

Printer-friendly Version

Interactive Discussion

## Tropospheric ozone retrievals from SCIAMACHY observations

F. Ebojje et al.

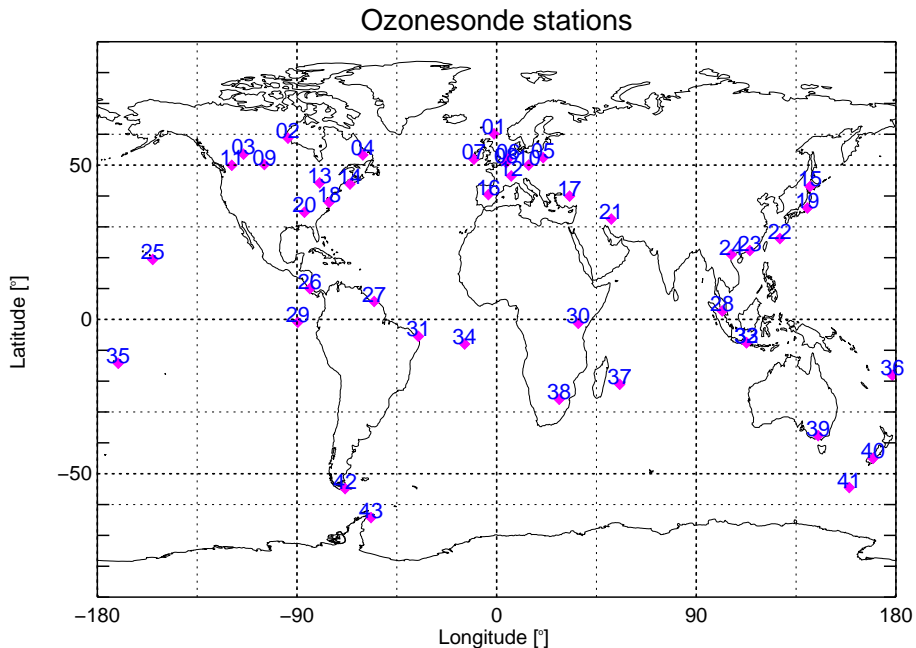


**Fig. 5.** World map showing ozonesonde stations (station numbers are listed in Table 4) used in this study.

[Title Page](#)

[Abstract](#)

[Introduction](#)

[Conclusions](#)

[References](#)

[Tables](#)

[Figures](#)

◀

▶

◀

▶

[Back](#)

[Close](#)

[Full Screen / Esc](#)

[Printer-friendly Version](#)

[Interactive Discussion](#)

## Tropospheric ozone retrievals from SCIAMACHY observations

F. Ebojie et al.

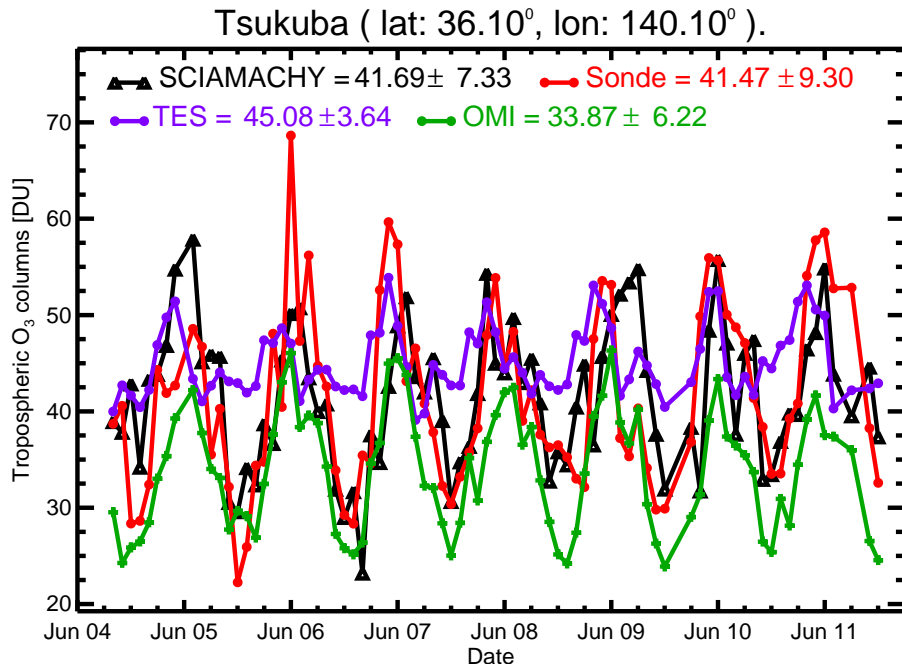


**Fig. 6.** Comparison of monthly mean tropospheric ozone column time series in Dobson Units (DU) between SCIAMACHY (black), ozonesondes (red), TES (violet), and OMI/MLS (green) over Tsukuba ( $36.10^{\circ}$  N,  $140.10^{\circ}$  E).

## Tropospheric ozone retrievals from SCIAMACHY observations

F. Ebojje et al.

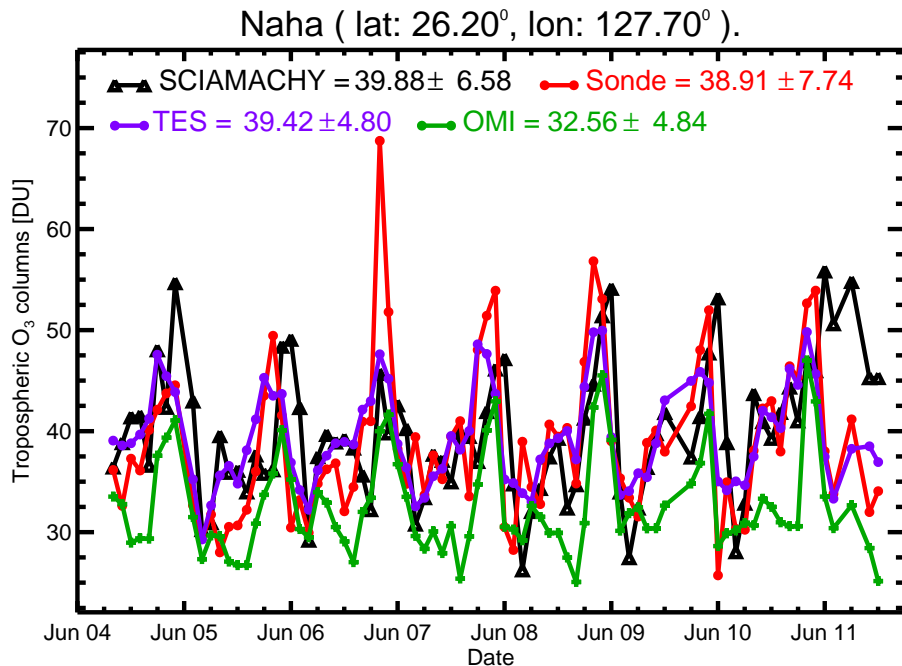


**Fig. 7.** Comparison of monthly mean tropospheric ozone column time series in Dobson Units (DU) between SCIAMACHY (black), ozonesondes (red), TES (violet), and OMI/MLS (green) over Naha ( $26.20^{\circ}$  N,  $127.70^{\circ}$  E).

## Tropospheric ozone retrievals from SCIAMACHY observations

F. Ebojje et al.

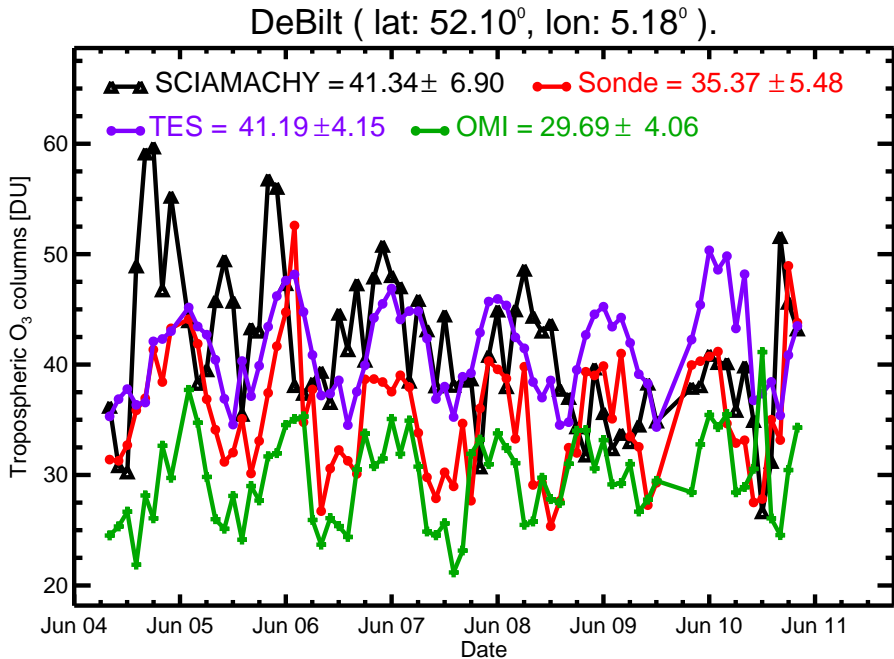


**Fig. 8.** Comparison of monthly mean tropospheric ozone column time series in Dobson Units (DU) between SCIAMACHY (black), ozonesondes (red), TES (violet), and OMI/MLS (green) over DeBilt ( $52.10^{\circ}$  N,  $5.18^{\circ}$  E).

- [Title Page](#)
- [Abstract](#) [Introduction](#)
- [Conclusions](#) [References](#)
- [Tables](#) [Figures](#)
- [◀](#) [▶](#)
- [◀](#) [▶](#)
- [Back](#) [Close](#)
- [Full Screen / Esc](#)

[Printer-friendly Version](#)

[Interactive Discussion](#)

## Tropospheric ozone retrievals from SCIAMACHY observations

F. Ebojje et al.

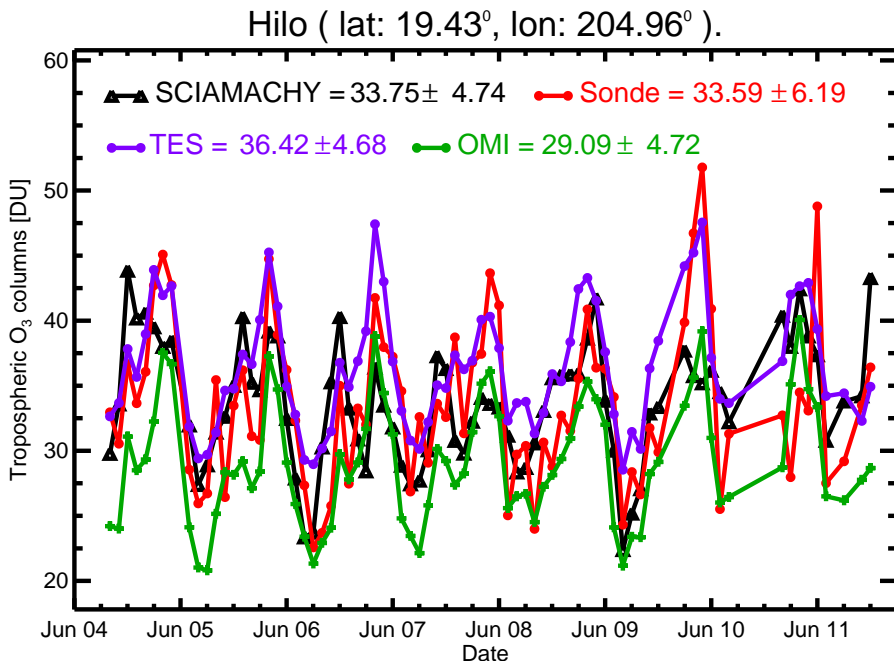


**Fig. 9.** Comparison of monthly mean tropospheric ozone column time series in Dobson Units (DU) between SCIAMACHY (black), ozonesondes (red), TES (violet), and OMI/MLS (green) over Hilo ( $19.72^{\circ}$  N,  $24.93^{\circ}$  W).

- [Title Page](#)
- [Abstract](#) [Introduction](#)
- [Conclusions](#) [References](#)
- [Tables](#) [Figures](#)
- [◀](#) [▶](#)
- [Back](#) [Close](#)
- [Full Screen / Esc](#)

[Printer-friendly Version](#)

[Interactive Discussion](#)

## Tropospheric ozone retrievals from SCIAMACHY observations

F. Ebojje et al.

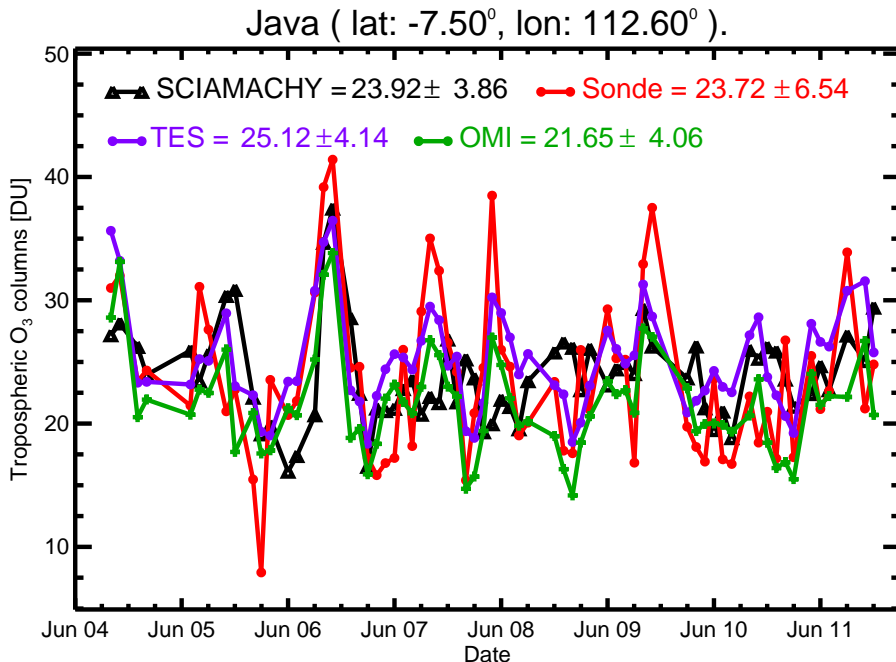


**Fig. 10.** Comparison of monthly mean tropospheric ozone column time series in Dobson Units (DU) between SCIAMACHY (black), ozonesondes (red), TES (violet), and OMI/MLS (green) over Java ( $7.50^{\circ}$  S,  $112.60^{\circ}$  E).

## Tropospheric ozone retrievals from SCIAMACHY observations

F. Ebojie et al.

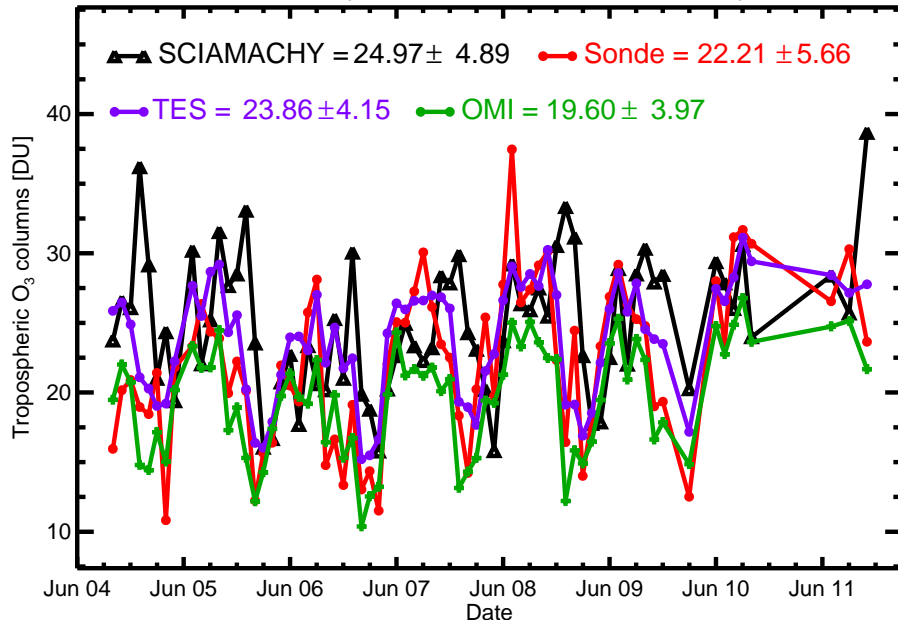


**Fig. 11.** Comparison of monthly mean tropospheric ozone column time series in Dobson Units (DU) between SCIAMACHY (black), ozonesondes (red), TES (violet), and OMI/MLS (green) over Samoa ( $14.23^{\circ}$  S,  $170.56^{\circ}$  W).

## Tropospheric ozone retrievals from SCIAMACHY observations

F. Ebojie et al.

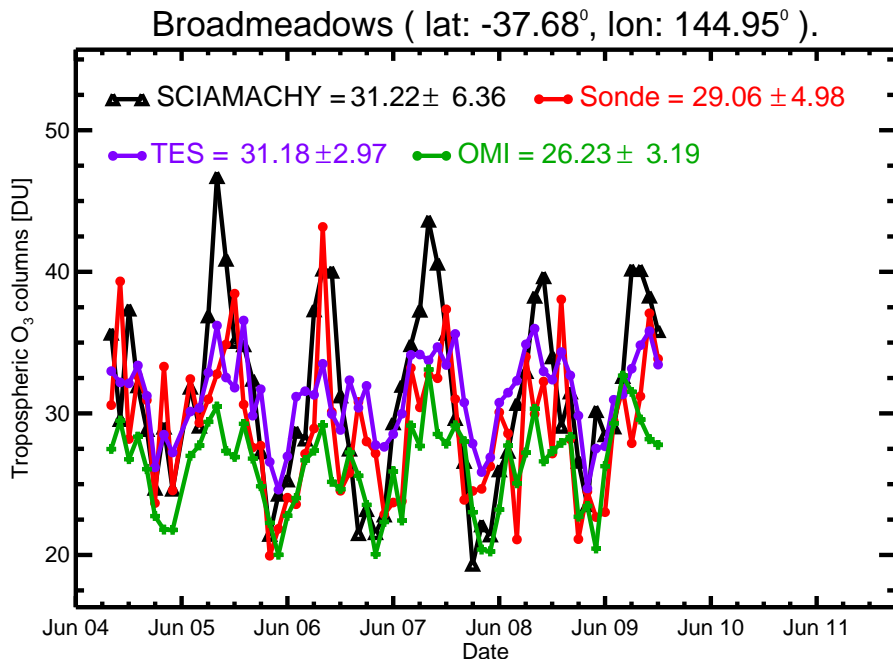


**Fig. 12.** Comparison of monthly mean tropospheric ozone column time series in Dobson Units (DU) between SCIAMACHY (black), ozonesondes (red), TES (violet), and OMI/MLS (green) over Broadmeadows ( $37.68^{\circ}$  S,  $144.95^{\circ}$  E).

- [Title Page](#)
- [Abstract](#) [Introduction](#)
- [Conclusions](#) [References](#)
- [Tables](#) [Figures](#)
- [◀](#) [▶](#)
- [◀](#) [▶](#)
- [Back](#) [Close](#)
- [Full Screen / Esc](#)

[Printer-friendly Version](#)

[Interactive Discussion](#)

## Tropospheric ozone retrievals from SCIAMACHY observations

F. Ebojie et al.

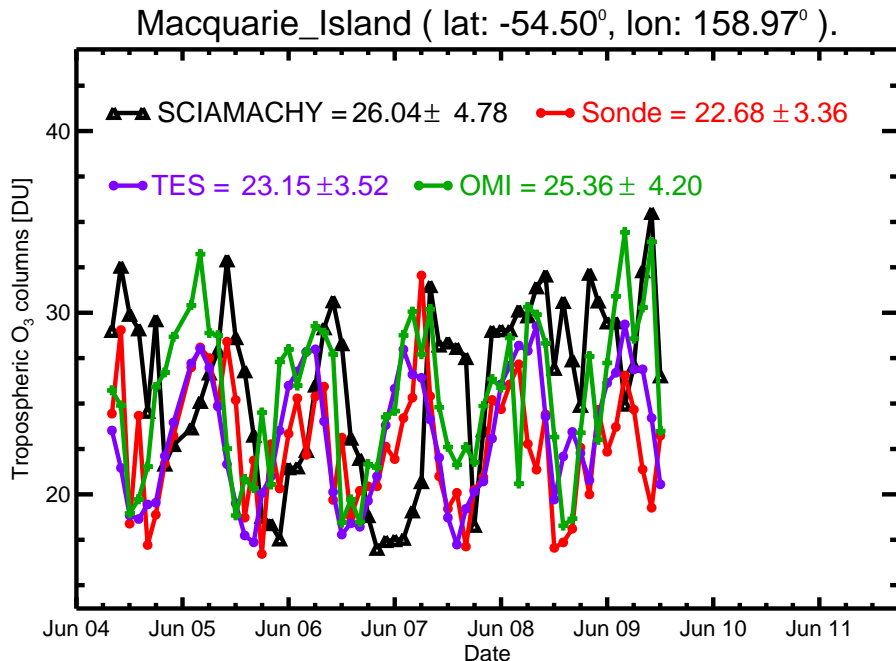


**Fig. 13.** Comparison of monthly mean tropospheric ozone column time series in Dobson Units (DU) between SCIAMACHY (black), ozonesondes (red), TES (violet), and OMI/MLS (green) over Macquarie Island ( $54.50^{\circ}\text{S}$ ,  $158.95^{\circ}\text{E}$ ).

## Tropospheric ozone retrievals from SCIAMACHY observations

F. Ebojie et al.

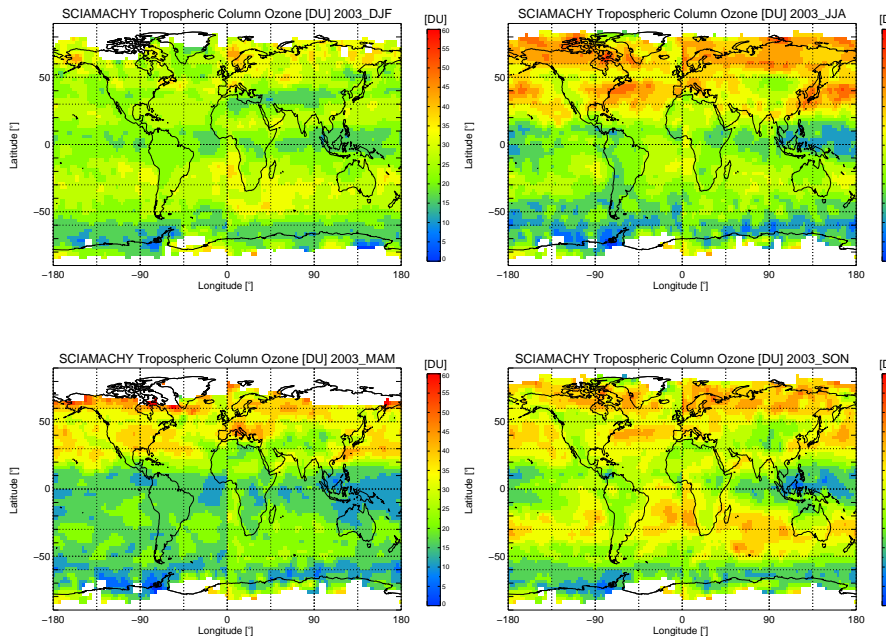


**Fig. 14.** Tropospheric ozone distributions in Dobson Units from SCIAMACHY for the different seasons in 2003; top panel from left to right: December–January–February, and June–July–August, bottom panel from left to right: March–April–May and September–October–November.

Title Page

Abstract

Introduction

Conclusions

References

Tables

Figures



Back

Close

Full Screen / Esc

Printer-friendly Version

Interactive Discussion

## Tropospheric ozone retrievals from SCIAMACHY observations

F. Ebojje et al.

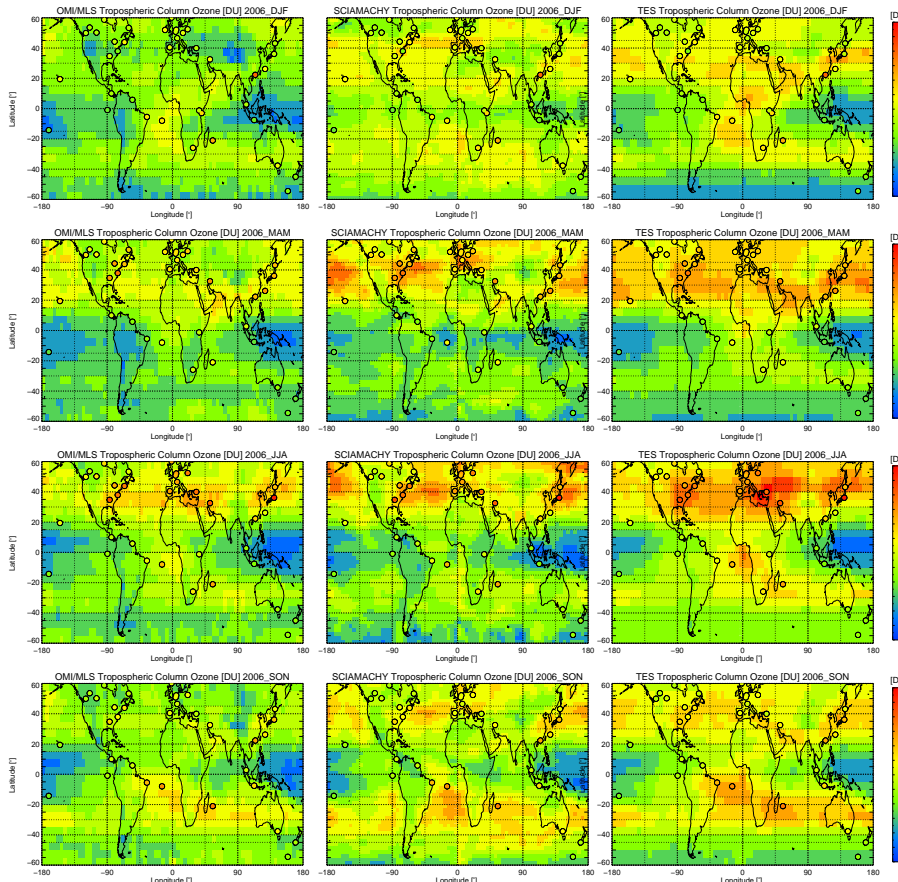


**Fig. 15.** Tropospheric ozone distributions in Dobson Units from left to right: OMI/MLS, SCIAMACHY and TES for different seasons in 2006, from the top panels to the bottom panels: December-January-February, March-April-May, June-July-August and September-October-November.

[Title Page](#)

[Abstract](#)

[Introduction](#)

[Conclusions](#)

[References](#)

[Tables](#)

[Figures](#)



[Back](#)

[Close](#)

[Full Screen / Esc](#)

[Printer-friendly Version](#)

[Interactive Discussion](#)